A microfluidics-based platform enables discovery of gametogenic rejuvenation factors in *Saccharomyces cerevisiae*

Silvan Spiri[1]*, Tina Lynn Sing[1], Nhi Phung[1], Jay S Goodman[4], Elçin Ünal[1,2,3]* & Gloria Ann Brar[1,2,3]*

[1]Department of Molecular and Cell Biology, University of California, Berkeley, Berkeley, CA, 94720, USA
[2]California Institute for Quantitative Biosciences (QB3), University of California, Berkeley, CA, 94720, USA
[3]Center for Computational Biology, University of California, Berkeley, Berkeley, CA 94720, USA
[4]Whitehead Institute for Biomedical Research, Massachusetts Institute of Technology, Cambridge, MA 02142, USA

*Correspondence: silvan.spiri@berkeley.edu, elcin@berkeley.edu, gabrar@berkeley.edu

Key words: *Saccharomyces cerevisiae*, meiosis, gametogenesis, cellular rejuvenation, replicative lifespan, microfluidics, autophagy.

Abstract

During mitotic growth, *Saccharomyces cerevisiae* cells age by dividing asymmetrically producing young daughter cells while retaining age-associated damage in the mother cell, which will eventually become senescent. Gametogenesis naturally and completely resets this replicative lifespan, even in replicative aged cells. Methods to quantify replicative lifespan resetting have been limited to low-throughput and labor-intensive approaches based on repeated manual micromanipulation of individual cells. Here, we introduce a high-throughput microfluidic-based assay that allows systematic characterization of factors required for gametogenic rejuvenation in *S. cerevisiae.* A key innovation of this method involves two inert genetic modifications that enable specific enrichment of gametes. With this technique, we confirm the rejuvenation of aged precursor cells upon completion of gametogenesis and show that we can capture a wide range of gamete replicative lifespan, consistent with known longevity mutants. Excitingly, using this technique, we identify factors involved in ER-phagy as essential for full restoration of replicative lifespan in gametes. We anticipate this novel technique will enable systematic identification of genes that mediate gametogenic rejuvenation.

Introduction

Life is continuously maintained by organisms through the genesis of offspring. In sexually reproducing eukaryotes, gametogenesis is a conserved developmental program that forms haploid gametes from diploid precursor cells. Although somatic cells deteriorate over time, mechanisms exists that eliminate age-associated damage in the germline and during gametogenesis to secure the fitness and survival of the next generation (Gladyshev, 2021; Jones, 2007; Maklakov and Immler, 2016; Smelick and Ahmed, 2005; Yamashita, 2023). Despite the importance of these pathways, the specific molecular mechanisms mediating this programmed developmental rejuvenation remain elusive.

During mitotic growth, *Saccharomyces cerevisiae* divides asymmetrically producing young daughter cells by retaining age-associated damage in the aging mother cell (Denoth Lippuner et al., 2014; Higuchi-Sanabria et al., 2014; Hughes and Gottschling, 2012; Nyström and Liu, 2014). This limits the number of daughter cells that a mother cell can produce (termed "replicative lifespan") before reaching senescence. Excitingly, upon completion of gametogenesis, replicative lifespan of all gametes completely resets in *S. cerevisiae*, relative to that of the precursor cell (Neiman, 2011; Sing et al., 2022; Ünal et al., 2011; Ünal and Amon, 2011) (**Fig. 1**). The portability of this rejuvenation program was demonstrated by the ability of ectopic expression of Ndt80, a transcription factor necessary for completion of gametogenesis, to extend replicative lifespan in mitotic cells (Ünal et al., 2011; Xu et al., 1995). Since this initial discovery, there has been growing interest in factors that are expressed during gametogenesis and that may drive lifespan resetting in gametes (Sing et al., 2022). Drug-mediated inhibition of autophagy prevents clearance of age associated Hsp104 foci during gametogenesis and completion of gametogenesis, suggesting that autophagy might play an important role in orchestrating gametogenic rejuvenation (Tyler and Johnson, 2018; Ünal et al., 2011).

Yeast gametogenesis, a highly experimentally tractable process that can be induced efficiently at will, presents the unique opportunity to gain mechanistic insights into the process of germline rejuvenation, but current techniques to quantify replicative lifespan of gametes limit progress in the field. Quantification of replicative lifespan in gametes has historically relied on scoring cell divisions using manual micromanipulation, with the replicative lifespan of a gamete mother cell being scored over several days by continuous counting and removing of daughter cells using a microdissection microscope (Ünal et al., 2011). This technique is tedious, time consuming and low throughput. In fact, since gametogenesis-specific rejuvenation was initially observed (Ünal et al., 2011), only one other study has used this technique to measure replicative lifespan of gametes (Lee et al., 2019) and no specific pathways that directly mediate gametogenic rejuvenation have been found. Although micromanipulation has historically been used to quantify replicative lifespan in vegetatively growing haploid yeast cells (Mortimer and Johnston, 1959), microfluidics-based approaches that increase throughput and lower manual labor have successfully been developed and adopted for yeast lifespan measurement in recent years. Multiple different trap designs have been used to capture and retain mother cells in imaging chambers with a constant media flow over prolonged periods of time. Parallelization of multiple imaging chambers allows acquisition of hundreds of cells from multiple different genetic backgrounds over a few days in one single experiment (Chen et al.,

2017; Jin et al., 2019; Jo et al., 2015; Li et al., 2020, 2017; Liu et al., 2015; Thayer et al., 2022). Although microfluidics-based quantification of replicative lifespan is rapidly replacing micromanipulation-based readouts for vegetatively growing haploid yeast cells, a technique to apply microfluidics-based platforms to specifically investigate the replicative lifespan of gametes does not currently exist. The challenges associated with capturing and measuring gamete lifespan include (i) the need to separate gametes from precursor cells and from the ascus that encloses four gametes together, (ii) the need to prevent mating of neighboring gametes, and (iii) the small size of gametes relative to precursor cells.

To overcome these limitations, we developed a microfluidic-based microscopy assay that allows high-throughput characterization of factors required for gametogenic rejuvenation in *S. cerevisiae*. Throughout this study we used the SK1 strain background, which undergoes gametogenesis with high efficiency and is the gold standard to study gametogenesis in yeast (Kane and Roth, 1974; Padmore et al., 1991; Williamson et al., 1983). During gametogenesis a diploid yeast cell undergoes two meiotic divisions forming a tightly packed tetrad containing four haploid gametes with a 2:2 segregation of the two mating types *MAT*a and *MAT*α (**Fig. 1** & **Fig. 3C**). To enable microfluidic-based assessment of replicative lifespan in *S. cerevisiae* gametes derived from the SK1 background, we first modified the base genotype to eliminate both covalent (mother-daughter cell adherence) and non-covalent (flocculation) interactions, rendering it more analogous to the lab-domesticated S288C strain. We also engineered a conditionally sterile allele that prevents post-germination mating without interfering with standard genetic crosses. Finally, we introduced a long-lived, gamete-specific fluorescent reporter that allowed for efficient identification and outgrowth of gametes compatible with microfluidic trapping. Using this system, we isolated single gametes from both young and aged precursor cells, loaded them into custom-designed microfluidic devices, and performed continuous time-lapse imaging over 72 hours. This approach enabled clear distinction between gametes and precursor cells, allowing quantitative analysis of gamete replicative lifespan.

Comparing the replicative lifespan of gametes derived from young versus aged precursor cells revealed, for the first time, that gametogenesis fully resets replicative lifespan in the SK1 strain background. Our platform captured a broad spectrum of lifespan outcomes and confirmed effects of known longevity mutants. Notably, using this system, we discovered that autophagy factors required for ER-phagy, are important for complete lifespan resetting in aged gametes. This technique substantially enhances the feasibility and throughput of lifespan analysis, enabling direct identification of molecular pathways that mediate cellular rejuvenation during gametogenesis. These advances are poised to uncover new mechanisms by which eukaryotic cells counteract age-associated damage.

Results

Pma2 is specifically expressed in gametes, localizes to the plasma membrane, and exhibits gamete-specific retention beyond germination.

PMA2, a paralogue of *PMA1*, encodes a plasma membrane proton pump known to regulate nutrient uptake, cytoplasmic pH and localizes to the periphery of the cell (Carmelo et al., 1997; Saliba et al., 2018; Serrano et al., 1986). Pma1 is highly expressed during vegetative growth, with an exceptionally long half-life displaying asymmetric retention in mother cells

(Henderson et al., 2014). While *PMA1* is essential for viability, *PMA2* is non-essential, and expressed at barely detectable levels during mitotic growth (Fernandes and Sá-Correia, 2003; Schlesser et al., 1988; Serrano et al., 1986). Interestingly, *PMA2* translation and protein levels are upregulated during late gametogenesis (Brar et al., 2012; Cheng et al., 2018). To further investigate the expression pattern of *PMA2*, we created a transgenic reporter strain carrying a Pma2-GFP fusion protein under its endogenous promoter and characterized its expression timing relative to meiotic divisions, which were tracked using a fluorescently labeled chromatin marker (Htb1-mCherry). Pma2-GFP expression was specifically upregulated 1-2 hours following anaphase II and Pma2-GFP predominantly localized to the gamete plasma membranes (**Fig. 2A**). Importantly, Pma2-GFP was not detected in cells that fail to undergo gametogenesis (arrows, **Fig. 2A**). Next, we analyzed Pma2-GFP expression in gametes undergoing germination, their first mitotic division. We found that daughter cells from gametes completely lacked Pma2-GFP signal and that Pma2-GFP was fully retained on the plasma membrane of gametes for several rounds of cell division (**Fig. 2B**). Our expression pattern analysis revealed that Pma2-GFP is a reliable and specific marker of gametes, making it an optimal reporter to distinguish gametes from vegetative cells or cells that fail to complete gametogenesis.

Cell populations efficiently sorted by age progress robustly through gametogenesis

To assess the ability of our approach to reliably quantify gametogenic rejuvenation, we first separated pre-meiotic diploid cell populations by replicative age using an established protocol (Smeal et al., 1996). Briefly, a founder cell population was biotin labelled with sulfo-NHS-LC-biotin, which specifically and permanently binds to cell surface proteins that are retained in the founder (mother) cells during subsequent mitotic divisions. These biotin-labeled founder cells were then replicatively aged and incubated with anti-biotin magnetic beads that enabled their isolation from the young daughter cells. The labeled cell suspension was passed through a magnetic column followed by elution and applied to a second column to increase purity. The first flow-through cells were collected as the young cell population. The eluate from the second column was collected and used as the aged cell population (**Fig. 2I**). Sorted cell populations were stained with a fluorophore conjugated to streptavidin and a second fluorophore conjugated to wheat germ agglutinin that specifically binds to chitin-rich, ring-like structures called bud scars on the yeast cell wall, one of which is left after each budding event thus revealing the replicative age of a cell (Cabib and Bowers, 1971). We measured the purity as well as the age of the sorted population by fluorescent microscopy to analyze biotin labelling and bud scar number in both cell populations (**Fig. 2C**, left panel). We found that with our consecutive-sort protocol, we consistently obtained young cell populations containing 3.63% biotinylated cells with a mean replicative age of 1.16, and aged cell populations containing 96.74% biotinylated cells with a mean replicative age of 8.55 (**Fig. 2E&F**). We transferred the separated cell populations to media that induce gametogenesis and analyzed efficiency of gametogenesis after 24 hours. We found that 79.8% of young cells and 78.89% of aged cells successfully completed gametogenesis, forming visibly distinct tetrads (**Fig. 2D**). We also confirmed that gametes from young as well as aged cell population both robustly expressed Pma2-GFP after completion of gametogenesis (**Fig. 2C**, right panel). Furthermore, we re-

evaluated the purity as well as the age of the sorted population and confirmed that upon completion of gametogenesis gametes from the young cell population still only had 13.38% biotinylated cells with a mean replicative age of 1.31, compared to gametes derived from the aged cell population with 97.34% biotinylated cells and a mean replicative age of 8.17 (**Fig. 2G&H**). In conclusion, we find that consecutive magnetic bead sorting allows efficient age separation of pre-meiotic cells. We show that both young and aged populations can progress efficiently through meiosis and robustly express *PMA2-GFP* once gametogenesis is completed (**Fig. 2I**). Furthermore, and importantly, there is no detectable negative effect of the here applied aging regime on the capability to complete gametogenesis efficiently.

Isolation of single gametes allows assessment of replicative lifespan via microfluidics-based imaging

To be able to assess replicative lifespan of yeast gametes using microfluidic devices we had to overcome three major obstacles. First, we had to circumvent initiation of mating of gametes with different mating types in response to mating pheromones, which leads to growth arrest and abnormal cell morphology. Second the four gametes within a tetrad do not separate during germination (**Fig. 2B**) rendering assessment of replicative lifespan impossible, thus we had to find a way to separate tetrads into single gametes before loading into the microfluidics imaging chambers. Third, separated gametes, which are significantly smaller than vegetative growing cells, do not fit into our custom-built U-traps for vegetatively growing haploid SK1 cells that are found in our microfluidics devices (**Fig S1** adapted from (Jo et al., 2015)).

Cells from the SK1 background are known to form both covalent (mother-daughter cell adherence) and non-covalent (flocculation) interactions, which present an issue when using microfluidics-based application due to elevated clogging. To mitigate this, we introduce a point mutation into the *AMN1* locus, a modulator of cell separation and mitotic exit. The $Amn1^{D368V}$ allele promotes efficient mother-daughter cell separation (Fang et al., 2018). We also deleted *FLO8*, a transcription factor required for flocculation (Kobayashi et al., 1996). Next, to avoid triggering the mating response among the gametes, we created a conditional sterile strain background in which we replaced the endogenous promoter of the mating response signaling scaffold gene *STE5* (Chol et al., 1994), with an anhydrotetracycline-inducible promoter (**Fig. 3A**) (Bellí et al., 1998). We confirmed sterility and inducible fertility by mixing *MAT*a and *MAT*α cells in a 1:1 ratio on control and anhydrotetracycline-containing plates and monitored the mating response by scoring diploid formation (**Fig. 3B**).

To obtain single gametes starting from tetrads and to disenrich for cells that did not proceed through gametogenesis, we first incubated post-sporulation cultures with zymolase. This enzyme specifically digests the cell wall of yeast, thus lysing non-gametes and weakening the ascus protecting the gametes (**Fig. 3C**). Next, we carefully sonicated the zymolase-treated tetrads to disassociate them into single gametes and confirmed detectability of the Pma2-GFP marker on single gametes by fluorescence microscopy (**Fig. 3C&D**).

When loading separated gametes directly into our custom microfluidics devices (**Fig S1A-D** adapted from (Jo et al., 2015)), designed for vegetative haploid cells, we observed that gametes were not retained in the traps due to their small size. To circumvent this issue, gametes were first grown in rich media (YDP with 2% glucose) for 3 hours following their separation,

which was long enough for them to increase in size but short enough to only allow the first cell division to occur (**Fig. S1E**). These gametes were then loaded into the microfluidic devices and an image of the whole region of interest was taken in the FITC and brightfield channel. By assessing Pma2-GFP expression, we could reliably determine if a trapped cell was a gamete, or a progeny cell generated during re-growth (**Fig. 3E**). Next to quantify replicative lifespan of gametes, brightfield images were acquired every 15 minutes over 72 hours, capturing every cell division (**Fig. 3F&G**). Together, these steps constitute a pipeline to isolate yeast tetrads and robustly separate sterile gametes, which allows for the quantification of their replicative lifespan potential using a high-throughput microfluidics-based imaging platform (**Fig. 3H**).

Wild-type gametes from aged precursor cells completely reset replicative lifespan during gametogenesis

It has previously been shown that replicative lifespan is completely reset after gametogenesis. This study used a micromanipulator continuously counting and removing daughter cells of gametes previously placed onto agar plates. Because the wild-type *AMN1* allele in SK1 causes the first daughter cell to remain adherent to the gamete after its initial mitotic division, gametogenic rejuvenation was assessed only in the W303 and A364a strain background (Ünal et al., 2011). Thus, we wanted to test if in SK1, an established strain background to study meiosis and gametogenesis in yeast, gametes also showed a complete reset of their replicative lifespan. We also intended to determine the robustness of our microfluidic approach to detect such resetting. Towards this end, we sorted diploid wild-type cells following our established protocol (**Fig. 2I**) and analyzed the replicative age of young and aged pre-gametogenic cell populations. We determined that young wild-type pre-gametogenic cell populations contained 1.5% biotinylated cells and had a mean replicative age of 0.72 in contrast to the aged wild-type population with 96.4% biotinylated cells and a mean replicative age of 7.8 (**Fig. 4A&B**). Separated cell populations were transferred to media inducing gametogenesis and after 24 hours 72.3% of young and 75.7% of aged wildtype cells successfully completed gametogenesis (**Fig. 4C**). Analyzing purity of sorting and replicative age in post-gametogenic tetrads revealed young wildtype tetrads contained 1.3% biotinylated tetrads with a mean replicative age of 1.3 and aged wild-type population had 94.9% biotinylated tetrads with mean replicative age of 7.8 (**Fig. 4D&E**). We acquired and quantified the replicative lifespan of gametes following our pipeline and found the median replicative lifespan for wildtype gametes from young precursor cells was 20 showing no significant difference compared to wild-type gametes from aged precursors which had a median replicative lifespan of 21 (**Fig. 4F**, p=0.5058, Log-rank (Mantel-cox)). These results show, for the first time in the SK1 strain background, that replicative lifespan is completely reset during gametogenesis, and confirms that our newly developed high-throughput microfluidic based pipeline can capture and quantify gametogenic rejuvenation.

Microfluidics-based analyses capture a wide range of gamete lifespan measurements among known longevity mutants

To test the sensitivity of our approach in detecting differences in replicative lifespan potential of gametes, we quantified lifespans of young gametes derived from known longevity mutant

backgrounds. Deletion of the gene encoding Sir2, a NAD^+- dependent histone deacetylase, is known to decrease replicative lifespan of yeast by approximately 50% due in part to loss of silencing rDNA locus leading to the generation and accumulation of extrachromosomal rDNA circles (Kaeberlein et al., 1999; Sinclair and Guarente, 1997). On the other hand, deletion of the gene encoding Fob1, an rDNA spacer replication fork barrier binding protein, is reported to extend lifespan in yeast by up to approximately 40%, due to fewer stalled replication forks leading to decreased rDNA recombination and thus fewer extrachromosomal rDNA circles (Defossez et al., 1999).

We sorted *sir2*Δ, wild-type, and *fob1*Δ diploid cells using our protocol (**Fig. 2I**) and analyzed the replicative age of the young pre-gametogenic cell populations. We determined that sorted young pre-gametogenesis *sir2*Δ cell populations contained no biotinylated cells and had a mean replicative age of 1.3, the wild-type population had 3.7% biotinylated cells with a mean replicative age of 1.2 and the *fob1*Δ population had 9.5% biotinylated cells with a mean replicative age of 1.9 (**Fig. 4G&H**). We transferred the separated cell populations to media that induces gametogenesis and found after 24 hours 87.3% of *sir2*Δ cells, 90.4% of wildtype cells and 73.7% of *fob1*Δ cells successfully completed gametogenesis (**Fig. 4I**). Analyzing purity of sorting and replicative age in tetrads showed that *sir2*Δ cell populations contained 3.4% biotinylated tetrads with a mean replicative age of 1.3, the wild-type population contained 17.3% biotinylated tetrads with mean replicative age of 1.4, and the *fob1*Δ population contained 3.8% biotinylated tetrads with a mean replicative age of 1.2 (**Fig. 4J&K**). Next, we separated the tetrads into single gametes and acquired their replicative lifespan over 72 hours (**Fig. 2I, Fig. S1**). We quantified the replicative lifespan of gametes and found the median replicative lifespan for gametes derived from young precursor *sir2*Δ cells to be 11, significantly lower than gametes derived from young wild-type cells, with a median lifespan of 21 (**Fig. 4L**, $p<0.0001$, Log-rank (Mantel-cox)). Gametes derived from young *fob1*Δ precursor cells, on the other hand, had a significantly increased median lifespan of 28 compared to wildtype (**Fig. 4L**, $p<0.0001$, Log-rank (Mantel-cox)). In conclusion the microfluidic platform and workflow that we developed can capture a range of gamete lifespans from young precursor cells with mutations in established longevity-linked genes.

Gametes lacking *SIR2* fail to reset replicative lifespan through a mechanism that is independent of gametogenesis

While testing our pipeline we serendipitously discovered that gametes derived from old *sir2*Δ precursor cells did not display completely reset of replicative lifespan. We sorted *sir2*Δ pre-gametogenic diploid cells into a young cell population containing no biotinylated cells with a mean replicative age of 1.3 (same data as shown in **Fig. 4G&H**) and an aged cell population containing only biotinylated cells with a mean replicative age of 7 (**Fig. 5A&B**). We determined that 87.3% (same data as shown in **Fig. 4I**) of the young population and 68.0% of old population completed gametogenesis after 24 hours (**Fig. 5C**). Post-gametogenic young *sir2*Δ cells had 3.4% (same data as shown in **Fig. 4J**) biotinylated tetrads with mean replicative age of 1.3 (same data as shown in **Fig. 4K**) and aged *sir2*Δ had 91.9% biotinylated tetrads with a mean replicative age of 6.6 (**Fig. 5D&E**). Quantifying the replicative lifespan of gametes derived from aged *sir2*Δ precursor cells revealed a median replicative lifespan of 8,

significantly lower than for gametes derived from young *sir2*Δ precursor cells, which had a median lifespan of 11 (same data as shown in **Fig. 4L**) (**Fig. 5F**, p<0.0001, Log-rank (Mantel-cox)).

To test whether ectopic expression of *SIR2* during gametogenesis can rescue the lack of replicative lifespan resetting observed in *sir2*Δ cells, we constructed *sir2*Δ strains that also house the *SIR2* ORF genomically inserted under the control of a *RIM4* promoter fragment, which is activated during gametogenesis (Deng and Saunders, 2001). We confirmed gametogenesis-specific expression by western blotting (**Fig. 5G**). We then sorted pre-gametogenic diploid *sir2*Δ cells carrying this rescue construct into a young cell population containing no biotinylated cells with a mean replicative age of 0.98 and an aged cell population containing 98.0% biotinylated cells with a mean replicative age of 9.1 (**Fig. 5H&I**). We determined that 84% of the young population and 81.7% of old population completed gametogenesis after 24h (**Fig. 5J**). Gametes derived from the young population had no biotinylated tetrads with mean replicative age of 0.72 and aged population had only biotinylated tetrads with a mean replicative age of 8.1 (**Fig. 5K&L**). Gametes derived from aged *pRIM4-SIR2 sir2*Δ precursor cells showed a median replicative lifespan of 10 still significantly lower than gametes derived from young *pRIM4-SIR2 sir2*Δ cells, with a median lifespan of 17 (**Fig. 4M**, p<0.0001, Log-rank (Mantel-cox)). We note a slightly increased replicative lifespan of gametes derived from both young and old *pRIM4-SIR2 sir2* precursor cells compared to those derived from *sir2*Δ cells, which may be due to residual Sir2 protein observed in late gametes that could carry over through the first cell divisions (**Fig. 5G**, right most band). In summary, we show that *sir2*Δ gametes do not completely reset their lifespan following gametogenesis, however, this phenotype cannot be rescued by providing Sir2 during gametogenesis. This suggests that aged *sir2*Δ cells might accumulate damage that cannot be cleared by the gametogenic rejuvenation program.

Atg32 is not necessary to reset replicative lifespan during gametogenesis

Autophagy pathways decline during aging leading to loss of proteostasis and accumulation of cellular damage. Artificially increasing autophagy factors can lead to lifespan extension (Hansen et al., 2018; Rubinsztein et al., 2011; Simonsen et al., 2008; Tyler and Johnson, 2018). In yeast, autophagy is essential for meiotic entry as well as progression, and dynamic upregulation of autophagy factors has been observed in previous studies (Otto et al., 2021; Ünal et al., 2011). Thus, we tested if cellular quality control via autophagy plays a direct role in gametogenic rejuvenation. To address this, we first investigated a potential role for Atg32, an autophagy receptor localized on the outer mitochondria membrane that mediates selective removal of damaged and excess mitochondria via mitophagy (Kanki et al., 2009b; Kondo-Okamoto et al., 2012; Okamoto et al., 2009). Atg32 is strongly upregulated in mid-meiosis (Cheng et al., 2018).

We deleted *ATG32* in diploid cells and tested their gametogenic rejuvenation potential. Sorting of pre-gametogenic cells resulted in a young population with no biotinylated cells with a mean replicative age of 1.3 and an aged cell population containing 98.4% biotinylated cells with a mean replicative age of 8.1 (**Fig. 6A&B**). We determined that 82.4% of the young population and 81.0% of the aged population completed gametogenesis (**Fig 6C**) and that the

young gamete population contained 1.4% biotinylated tetrads and had a mean replicative age of 0.93 and aged gamete population had 97.0% biotinylated tetrads with a mean replicative age of 8.7 (**Fig. 6D&E**). Upon quantification of the replicative lifespan of gametes from young and aged precursor populations, no significant difference was observed with a median replicative lifespan of 22 from aged and 23 from young *atg32*Δ precursor cells (**Fig. 6F**, p=0.2691, Log-rank (Mantel-cox)). This result suggests that Atg32-mediated mitochondrial quality control via autophagy is dispensable for gametogenic rejuvenation of gametes from aged precursor cells.

ER-phagy is necessary for full gametogenic lifespan resetting

It has previously been shown that selective autophagy mediated by the autophagy receptors Atg40, and Atg39 to a lesser extent, controls ER inheritance during gametogenesis. Meiotic remodeling of the ER combined with ER-phagy prevent specific subpopulations of the ER from being passed onto gametes. It has been proposed that these pathways contribute to a quality control mechanism to ensure gametogenic rejuvenation, however this has not been directly tested (Otto et al., 2021; Otto and Brar, 2022).

To determine if Atg39, a transmembrane autophagy receptor in the perinuclear ER mediating nucleophagy (Mochida et al., 2015) impacts gametogenic rejuvenation, we first sorted diploid *atg39*Δ cells into a young population with 3.5% biotinylated cells with a mean replicative age of 0.98 and an aged cell population with only biotinylated cells and a mean replicative age of 8.1 (**Fig. 7A&B**). In the young and old populations, 70.0% and 82.0% completed gametogenesis, respectively (**Fig 7C**). Post-gametogenesis we found the young population had 2.0% biotinylated tetrads and a mean replicative age of 1.3 while the aged population had only biotinylated tetrads with a mean replicative age of 8.1 (**Fig. 7D&E**). Quantifying the replicative lifespan of gametes showed no significant difference for *atg39*Δ gametes derived from aged precursors with a median replicative lifespan of 23 and *atg39*Δ gametes derived from young precursors with a median lifespan of 22 (**Fig. 7F**, p=0.418, Log-rank (Mantel-cox)).

Next, we checked if gametogenic reset of replicative lifespan is impaired in cells lacking Atg40, an autophagy receptor localized at the cortical and cytoplasmic ER mediating fragmentation and encapsulation of ER subdomains (Mochida et al., 2015). *atg40*Δ diploid cells were age-sorted before gametogenesis resulting in a young cell population containing 11.9% biotinylated cells with a mean replicative age of 1.6 and an aged population with only biotinylated cells and a mean replicative age of 9.3 (**Fig. 7G&H**). Efficiency of gametogenesis of the young population was 78.7% and 78.0% for the old cell population (**Fig. 7I**). Post-gametogenesis, the gamete population derived from young cells had 8.9% biotinylated tetrads with a mean replicative age of 1.4, while the aged cell population had 98.1% biotinylated tetrads with and a mean replicative age of 8.6 **(Fig 7J&K**). Like *atg39*Δ cells, no significant difference in replicative lifespan was observed between *atg40*Δ gametes derived from aged precursors that had a median replicative lifespan of 23 and *atg40*Δ gametes derived from young precursors that had a median lifespan of 22 (**Fig. 7L**, p=0.389, Log-rank (Mantel-cox)).

There is known functional redundancy between Atg39 and Atg40 and it was previously observed that deletion of *ATG39* can exacerbate meiotic *atg40*Δ phenotypes (Mochida et al., 2015; Otto et al., 2021). Thus, we tested if *atg39*Δ *atg40*Δ cells were capable of completely

resetting replicative lifespan during gametogenesis. After sorting *atg39*Δ *atg40*Δ diploid cells into young and aged populations, we found that there were no biotinylated cells in the young cell population resulting in a mean replicative age of 1.4 and that 98.6% of cells in the aged population where biotinylated with a mean replicative age of 9.1 (**Fig. 8A&B**, Rep.1). 80.7% of the young precursor population and 75.3% of the aged precursor population completed gametogenesis, respectively (**Fig. 8C**, Rep.1). Post-gametogenesis, the young precursor population had no biotinylated tetrads with a mean replicative age of 1.1, all tetrads of the aged precursor population were biotinylated, with a mean replicative age of 8.6 (**Fig 8D&E**, Rep.1). Excitingly, lifespan analysis of gametes from aged *atg39*Δ *atg40*Δ precursor cells revealed a significantly reduced median replicative lifespan of 23 compared to gametes from young precursor cells with a median lifespan of 24 (**Fig 8F**, Rep.1, p=0.0017, Log-rank (Mantel-cox)). We repeated this experiment, sorting pre-gametogenic cells into a young cell population containing no biotinylated cells and a mean replicative age of 1 and aged cell population with 98.8% biotinylated cells with a mean replicative age of 8.7 (**Fig. 8A&B**, Rep.2). 85.3 of the young and 76.0% of the aged population completed gametogenesis (**Fig. 8C**, Rep.2). The young cell population had 1.2% biotinylated tetrads and a mean replicative age of 1.1, while all tetrads of the aged population where biotinylated with a mean replicative age of 9.4 (**Fig 8D&E**, Rep.2). Lifespan analysis showed again a similar significant lower median replicative lifespan of 22 in gametes from aged precursor *atg39*Δ *atg40*Δ cells compared to gametes from young precursor cells with a median lifespan of 24 (**Fig. 8F**, Rep.2, p=0.0080, Log-rank (Mantel-cox)). Together, these data revealed that Atg39 and Atg40 both contribute through partially redundant mechanisms to gametogenic rejuvenation, and that full replicative lifespan resetting during gametogenesis depends on the presence of these ER-phagy receptors.

Discussion

Here we present a new method to assess the molecular mechanisms underlying the natural cellular rejuvenation that accompanies gametogenesis using a high throughput microfluidics platform in budding yeast cells. This technique accelerates investigations of gametogenic rejuvenation efficiency in diverse genetic backgrounds and will be crucial to reveal further mechanistic insights into the conserved process of gametogenic rejuvenation. Using our microfluidics-based platform, we show here for the first time that replicative lifespan completely resets after gametogenesis in the SK1 strain background, corroborating previous reports that described and characterized this phenomenon in other strain backgrounds using microdissection assays as a readout (Ünal et al., 2011). Analysis of gamete lifespan in known longevity mutants reveals a large dynamic range of measurement using this approach. We found that in *sir2*Δ gametes from aged precursor cells, replicative lifespan was not fully reset due to a gametogenesis-independent mechanism. Finally, we revealed that in contrast to Atg32 an autophagy receptor involved in mitophagy, the combined function of Atg39 and Atg40, two ER associated selective autophagy receptors, is essential to completely reset replicative lifespan of aged gametes.

The custom microfluidic devices presented here, with an open U-trap design, can capture a wide dynamic range of replicative lifespan with lower confinement of cells in space compared to other trap designs that can lead to negative effects on longevity due to compression

of cells (Gao et al., 2020). This open design presents the drawback that cells might undergo ejection prematurely before senescence can be observed, due to either a significant increase of cell size during the last few divisions of replicative life or due to minor pressure aberrations in the fluidics system over time. To avoid biases when evaluating replicative lifespan of gametes, we counted every gamete that was loaded at the start of our time lapse and classified cells that ejected as censored subjects during analysis (see methods). Following this approach, we can consistently and robustly measure replicative lifespan. We find that ejection rates tend to increase specifically in lifespan extending mutants rendering such readouts noisier, but still the quantified increase of 33.33% in median lifespan of young *fob1*Δ gametes compared to lifespan of young wild-type gametes is within the range of previous reports (Defossez et al., 1999; Kaeberlein et al., 2004). To mitigate ejections in future experiments, devices with novel trap designs are being currently developed and tested.

SIR2 is a well characterized conserved histone deacetylase of the Sirtuin family and regulates replicative lifespan, amongst other functions, by silencing the ribosomal DNA locus (Kaeberlein et al., 1999; Sinclair and Guarente, 1997). Deletion of the *SIR2* leads to a significant decrease of replicative lifespan due elevated extrachromosomal rDNA circles and copy number amplification of specific chromosome regions (Foss et al., 2017; Hoggard et al., 2018; Hotz et al., 2022; Kaeberlein et al., 1999; Kobayashi et al., 2004; Sinclair and Guarente, 1997). This is caused by failure to repress increased double strand breaks at the rDNA locus due to *FOB1* mediated replication fork stalling and decreased recruitment of cohesion, both leading to increased rDNA recombination and broad chromosome instabilities due to destabilization of the rDNA locus (Ide et al., 2010; Kobayashi et al., 2004; Kobayashi and Ganley, 2005). Our results show that gametes from aged *sir2*Δ precursor cells failed to reset replicative lifespan, a phenotype that could not be rescued by gametogenesis-specific expression of Sir2. One plausible explanation for this is that due to elevated recombination, aged *sir2*Δ cells accumulate chromosomal aberrations, which cannot be corrected during gametogenesis, and are propagated to gametes, thus reducing their life expectancy.

The mammalian homologue SIRT1 and to a lesser degree *SIR2* in yeast have been suggested to play a role in regulating mitophagy (Lee et al., 2013, 2008; Sampaio-Marques et al., 2012), autophagy-mediated degradation of damaged and unnecessary mitochondria. In yeast, *ATG32* is a selective autophagy receptor localized on the outer mitochondria membrane (Kanki et al., 2009b; Okamoto et al., 2009). Specific mitochondrial remodeling and inheritance during gametogenesis has been described (Sawyer et al., 2018; Suda et al., 2007). However, gametes from aged *atg32*Δ precursor cells completely reset replicative lifespan, confirming that Atg32-mediated selective autophagy is not necessary for gametogenic rejuvenation. *ATG33* is an additional factor required for selective autophagy of mitochondria in yeast (Kanki et al., 2009a). It is plausible that either Atg33 or the combined function of Atg32 and Atg33, as seen with Atg39 and Atg40 for Er-phagy, mediates gametogenic rejuvenation via mitophagy. Alternately, autophagy-independent mechanisms may secure mitochondrial quality control during gametogenesis. Both scenarios will be interesting to address in future studies using our method.

Developmentally programmed ER remodeling followed by selective autophagy of ER components regulates ER inheritance during yeast gametogenesis (Otto et al., 2021; Otto and

Brar, 2022). ER-specific autophagy receptors Atg40 and Atg39, localized on the cortical ER and perinuclear ER, respectively, control this process (Mochida et al., 2015). *atg40*Δ but not *atg39*Δ cells fail to degrade cortical ER components via autophagy during gametogenesis and *atg39*Δ cells show reduced autophagy-mediated loss of cortical and perinuclear ER proteins. Intriguingly, *atg40*Δ *atg39*Δ double mutants have an additive effect on ER protein degradation (Otto et al., 2021). We show that aged *atg40*Δ *atg39*Δ precursor cells fail to produce gametes with a fully reset lifespan. This could be caused by the failure to clear damaged and aggregated ER components accumulated in old cells, an interesting area to investigate in future studies.

The technique presented here significantly increases feasibility and throughput to identify molecular factors that mediate cellular rejuvenation during gametogenesis in budding yeast cells, thereby enabling new insights into this conserved process. To gain a more mechanistic and temporal understanding, this assay can easily be combined with auxin inducible degradation of factors of interest and simultaneous imaging of established aging biomarkers in gametes that fail to completely rejuvenate. An important future goal will be to test if newly identified rejuvenation factors that control gamete quality can also be transported to extend replicative lifespan in mitotic cells and, and if they have a conserved function in combating aging in other systems.

Materials and Methods

Yeast strains and plasmids:

Standard molecular methods were used to transform and generate all yeast strains, which were derived from the SK1 background. Specific genotypes, plasmids and primers used to generate strains are listed in **Table 1**. Deletions were generated by homology directed replacement of ORFs with selection cassettes (Longtine et al., 1998; Powers et al., 2022). The *pPMA2-Pma2-GFP* transgene plasmid was generated by Gibson assembly of the *PMA2* promoter and ORF region, amplified from genomic DNA, with an in frame *GFP*-containing *TRP1* single integration vector (Gibson et al., 2009). The *pTet07.1-STE5* promoter swap was generated by amplifying a *NatR-Tet07.1* fragment using primers that introduced homology for the *STE5* locus (Bellí et al., 1998; Longtine et al., 1998). The *pPRIM4-SIR2-V5* rescue construct was generated by Gibson assembly of the *SIR2* ORF region with *pRIM4* and *V5* containing *LEU2* single integration vector (Gibson et al., 2009). Generated plasmids were assembled using Hifi DNA assembly mix (NEbuilder Hifi DNA Assembly Master Mix, E2621L). Single integration plasmids were linearized with PmeI (New England Biolabs) mediated restriction digest before transformations and integrations were verified by PCR and sanger sequencing. Generated strains and plasmids are available upon request.

Media and growth conditions

Unless otherwise indicated, diploid cells were grown in YPD (1% yeast extract, 2% peptone, 2% glucose, 22.4 mg/L uracil, and 80 mg/L tryptophan). To induce gametogenesis cells were transferred to conditioned sporulation media containing 2% potassium acetate, amino acid supplements and ampicillin (40 mg/L adenine, 40 mg/L uracil, 10 mg/L histidine, 10 mg/L leucine and 10 mg/L tryptophan, 100 µg/mL ampicillin) at an OD_{600} of 0.8. All meiotic cultures were incubated on a shaker for 24h at 30°C to complete gametogenesis. To increase efficiency of gametogenesis, conditioned sporulation media was obtained by filter sterilizing a meiotic culture at 1.85 OD_{600} after 5 hours at 30°C and was stored at 4°C. For immunoblotting saturated YPD 2% cultures were re-diluted to 0.2 OD_{600} in BYTA (1% yeast extract, 2% bacto tryptone, 1% potassium acetate, and 50mM potassium phthalate) containing acetate as a carbon source and then grown overnight to saturation at 30°C before transfer to unconditioned sporulation media without ampicillin at an OD_{600} of 1.85.

Fluorescent Microscopy

Bud scar staining and Pma2-GFP expression patterns during meiosis and gamete maturation were visualized using a DeltaVision Elite wide-field fluorescence microscope (GE Healthcare), equipped with a 60x/1.42 NA oil-immersion objective. Images were deconvolved with softWoRx imaging software (GE Healthcare). Time lapse images were acquired using a CellAsics system as previously described (King et al., 2019).
Replicative lifespan timelapse imaging was performed using an ECHO Revolution (RON-K) microscope equipped with an Olympus 40x/1.4 NA oil-immersion objective.

Age sorting of pre-gametogenic yeast cells

Young and aged cell populations were sorted by biotin-labeling of a founder population followed by bead-mediated magnetic sorting (Smeal et al., 1996). First, a patch of diploid cells was inoculated in YPD (2%) and grown overnight shaking at room temperature until saturation. Cells were then re-diluted in YPD (2%) to an OD_{600} of 0.2 and grown at 30°C to an OD_{600} of 0.6-1. To increase yield, 2 x 8 OD_{600} units were harvested per genotype, washed 3x with PBS (pH 8), and then were transferred into PBS (pH 8) containing 2 mg/mL EZ-Link Sulfo-NHS-LC-biotin (ThermoFisher Scientific). Cells were vortexed for one minute and incubated for 30 minutes at 4°C on a nutator, washed 4 times with PBS + glycine (pH 8 + 100 mM glycine), and then washed once with YPD 2% before being added to two separate 500 mL flasks containing 50 mL YPD 2% + ampicillin (100 µg/mL) each. Biotin labeled cultures were aged for 15-19h shaking at 30°C. Aged cell cultures were pelleted, washed once with 20 mL PBS (pH 7.4 + 0.5% BSA), and then resuspended in 20 mL PBS (pH 7.4 + 0.5%) BSA containing 100 µL of anti-biotin magnetic beads (Miltenyi Biotechnology). Cells were incubated for 15 min at 4°C and mixed regularly by inversion, washed once with 20 mL PBS (pH 7.4 + 0.5% BSA) and then resuspended in 5 mL PBS (pH 7.4 + 0.5% BSA). Using a QuadroMacs sorter, both suspensions were applied to a column each. The first flowthrough from each column was collected, combined, and used as the young cell population. Each column was washed 4 times with 3 mL PBS (pH 7.4 + 0.5% BSA) before eluting into a second column, to increase purity. The second columns were washed three times with 3 mL PBS (pH 7.4 + 0.5% BSA), cells were eluted, combined, and subsequently used as the aged cell population.

Immunostaining and gametogenesis

Young and aged cell suspensions were washed twice with 12 mL PBS (pH 7) and resuspended in 4 mL PBS (pH 7). 4 µL of Wheat Germ Agglutinin, Alexa 350 Fluor conjugate (1 µg/mL, ThermoFisher Scientific) and anti-streptavidin (564 nm) (1 µg/mL) was added respectively and incubated for 15 minutes in the dark at room temperature. Cells where washed (3x) with 12 mL of unconditioned sporulation media and resuspended to an OD_{600} of 0.8 in conditioned sporulation media + ampicillin (100 µg/mL). 0.1 OD_{600} units of cells was fixed in 3.7% formaldehyde to assess age before gametogenesis. Cultures were incubated for 24 hours at 30°C in the dark to complete gametogenesis and a 0.1 OD_{600} units of cells were used directly to count tetrad formation and another fraction of cells were fixed in 3.7% formaldehyde to assess age post-gametogenesis by imaging and counting biotinylated cells as well as bud scars.

Tetrad separation into single gametes and re-growth

Post gametogenic age sorted cultures were pelleted and resuspended in 900 µL H_2O, 100 µL Zymolase (1 mg/mL) and 2 µL B-mercaptoethanol and the suspension was incubated for 3 hours on a nutator at 30°C. Cells were washed (1x) with H_2O and resuspended in 1 mL H_2O followed by repeated sonication (6x 20 seconds) incubating the cells 2-3 minutes on ice in-between sonication cycles. Upon tetrad separation, separated gametes were filtered (30 µm Pre-separation filter, militenyibiotec) and diluted in YPD 2% + ampicillin (100 µg/mL) to an OD_{600} of 0.8. After 3 hours at incubation on a nutator at 30°C, 1 mL of cell suspension was aliquoted, sonicated briefly for 5 seconds and filtered before loading into the microfluidics system.

Microfluidics loading and timelapse imaging of replicative lifespan

Microfluidics devices (**Fig S1** adapted from (Jo et al., 2015);18++ chips from iBiochips) were setup using the manufacturer's recommendations on an ECHO Revolution fluorescence microscope in the inverted position with the environmental chamber set to 30˚C. Briefly, 20 mL syringes (Becton, Dickinson and Company) were filled with ~15 mL of YPD 2% + ampicillin (100 µg/mL) + 1% Pluronic F-127 (P2443, Sigma), and then connected to a Clay Adams Intramedic Luer-Stub Adapter (Becton, Dickinson and Company). Non-DEHP Medical Grade Tubing (iBiochips, MTB-100, ID = 0.202", OD = 0.060", wall = 0.20") equipped with a hollow stainless-steel pin (iBiochips, HSP-200) was then used to connect the media syringe to the imaging units using the "media loading" ports. "Cell loading" ports were plugged with solid stainless-steel pins (iBiochips, SSP-200) while imaging units were primed with media for at least 2 hours with a flow rate of 2.4 µL/min using micropumps (iBiochips,78-7200BIO). After all units were filled with media, pumps were stopped an hour prior to cell loading. For cell loading, 5 mL syringes (Becton, Dickinson and Company) with Clay Adams Intramedic Luer-Stub Adapter (Becton, Dickinson and Company) were filled with cells diluted to an OD_{600} of 0.8 in YPD 2% + ampicillin (100 µg/mL). Solid stainless-steel pins were then removed from the "cell loading" ports and tubing and open stainless-steel pins were used to connect the syringe containing cells with the microfluidic device. Cells were loaded manually and, once sufficient cells were loaded, the "cell loading" ports were plugged with solid stainless-steel pins and media flow was resumed at 2.4 µL/min.

Timelapse imaging was performed using an Olympus 40x/1.4 NA oil-immersion objective an intended intervals of 15-20 minutes for 72 hours. The x-, y-, and z-motors were set to medium speed; however, varying stage speeds caused sporadic differences in imaging intervals. Thus, the recorded acquisition time provides accurate timing information. For each chamber, 2x27 images and three z-slices per position with 3-5 µm spacing, to compensate for focal plane differences across a single unit, were acquired. Autofocus was set across a 20 µm range with 0.2 µm spacing using the "Course-Fine" setting (Threshold = 4, Contrast Limit = 4). The XY Stage and Z Motor were both set to medium speed and Hyperscan was enabled for the "BF" channel using "Y-Axis" Axis Priority and "Bi" Scanning Pattern.

Quantification of replicative age and purity of sorted cells

Z-stacks (36, 0.2 µm spacing) of fixed young and aged cells/tetrads were acquired on a DeltaVision Elite wide-field fluorescence microscope (GE Healthcare), using a 60x/1.42 NA oil-immersion objective and deconvolved with softWoRx imaging software (GE Healthcare). To reliably count number of bud scars, images were cropped, 3D projected and counted using a custom semi-automated FIJI script (ImageJ2, V. 2.14.0/1.54m, (Schindelin et al., 2012)). Max intensity Z-projections were generated and displayed as examples in figures.

Quantification of gamete replicative lifespan

After the movie was completed, the ECHO batch exporter tool was used to export stitched TIFF images. Individual TIFF images were converted to 8-bit using FIJI (ImageJ2, V. 2.14.0/1.54m, (Schindelin et al., 2012)), then full chamber movies could be opened using the "Bio Formats Import" tool with the "Group files with similar names" box checked. Single

Pma2-GFP positive cells (gametes) were identified by eye and cropped both in the FITC image and the brightfield time course using a custom semi-automated FIJI script. Next using a semi-automated FIJI script, the replicative lifespan of Pma2-GFP positive cells (gametes) identified in the FITC image were counted, verifying identity by comparing the FITC and brightfield time-lapse for each single gamete. If a cell ejected from the U-trap before senescence was observed, this was noted and treated as a censored subject for quantification. For most experiments, counts from two technical replicates were concatenated unless otherwise indicated. Although throughput to quantify gametogenic reset of lifespan is significantly higher than with previous methods, cell divisions of each gamete must still be counted manually by a trained scientist rendering data analysis as a current bottleneck of the presented method.

Immunoblotting

For each sample, 10 OD_{600} units were harvested and pelleted from either log-phase YPD 2%, saturated YPD 2%, saturated BYTA or indicated timepoints upon transfer to sporulation media. For each sample, 2 mL 5% trichloroacetic acid was added and cells were incubated for ≥10 minutes at 4°C minutes, washed (1x) with acetone, and pellets was dried overnight. For protein extraction, ~100 µL glass beads and 100 µL of lysis buffer (50 mM Tris-HCl pH 8.0, 1 mM EDTA, 3 mM DTT, 2.2 mM PMSF, 1x complete EDTA-free inhibitor cocktail (Roche)) were added to the dried pellets and transferred to a Mini-Beadbeater-96 (BioSpec) for 5 minutes. Fifty µL of 3X SDS sample buffer (187.5 mM Tris pH 6.8, 6% β-mercaptoethanol, 30% glycerol, 9% SDS, 0.05% bromophenol blue) was added and samples were for boiled for 5 minutes at 95°C. Polyacrylamide gel electrophoresis (4–12% Bis-Tris Bolt gels, Thermo Fisher) and semi-dry transfer (Trans-Blot Turbo Transfer System, Bio-Rad) onto nitrocellulose membranes apparatus was used to separate and visualize proteins respectively. Odyssey PBS Blocking Buffer (LI-COR Biosciences) was used to block membranes (90 minutes, room temperature), and membranes were incubated overnight at 4°C with a mouse anti-3v5 (R960-25; RRID: AB_2556564, Thermo Fisher) antibody at 1:2000 in PBS +0.1% Tween-20 and a rabbit anti-Hx2k (RRID:AB_219918, 100–4159, Rockland) at 1:20000 in PBS +0.1% tween. Membranes were washed with PBS+ 0.1% Tween-20 (4x, 5 minutes each) and incubated with secondary antibody solutions containing anti-mouse conjugated to IRDye 800CW at a 1:15,000 dilution (RRID:AB_621847, 926–32212, LI-COR Biosciences) and an anti-rabbit conjugated to IRDye 680RD at a 1:15,000 dilution (RRID:AB_10956166, 926–68071, LI-COR Biosciences) in PBS +0.1% Tween-20. Membranes were imaged using an Odyssey CLx system (LI-COR Biosciences).

Statistical analysis

Prism Graphpad (version 10.1.0) was used to plot and analyze data. Prism Graphpad was used to calculated mean and standard deviation of replicative ages and to assess statistical significance in differences between replicative lifespans using the Log-rank (Mantel-cox) test. A Python script was used to calculated 95% confidence intervals using the Wilson score method.

Acknowledgements

We thank the current and former members of the Brar and Ünal laboratory for critical discussion and comments on the manuscript. This work is supported by the Swiss National Science Foundation mobility fellowship P500PB_214421 to S.S., G.B. is supported by funding from the National Institutes of Health (1R01AG071869 and 1R35GM134886) and the Astera Fund, TLS was supported by a Longevity Impetus Grant from the Norn Group, Hevolution Foundation and Rosenkranz Foundation. E.Ü. is supported by funding from the National Institutes of Health (R01AG071801) and the Astera Institute.

Author contributions

S.S. and N.P. performed experiments, S.S. and N.P. analyzed the data, S.S., T.L.S., N.P., J.S.G., E.Ü., G.A.B., wrote and edited the manuscript.

Declaration of interests:

The authors declare no competing interests.

Figures & Figure Legends

Figure 1

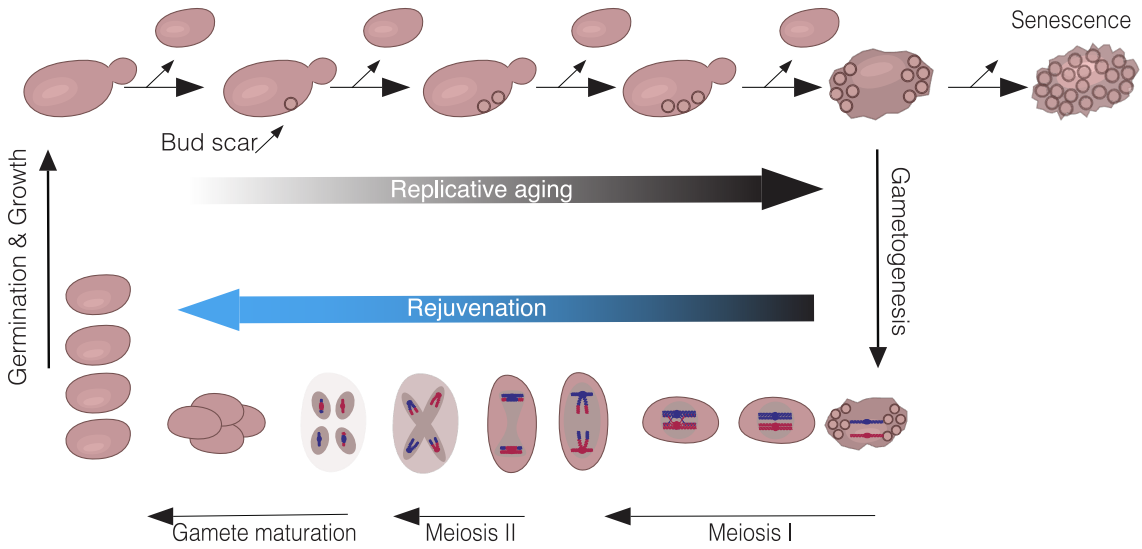

Figure 1. Replicative lifecycle and gametogenic rejuvenation in *Saccharomyces cerevisiae*. In vegetative growth, yeast divides asymmetrically where the daughter cell is born young while the mother cell accumulates aged and damaged components until reaching senescence. Replicative age of a single yeast cell is determined by the number of bud scars, which form at each division and are retained on the cell wall (top panel). Gametogenesis can be induced by nutrient depletion (downwards arrow, right). During gametogenesis, diploid yeast divides symmetrically, fully resetting their lifespan leading to the formation of four equally young haploid gametes, even from aged precursor cells (bottom panel). Addition of nutrients induces germination and return to mitotic growth (upward arrow, left).

Figure 2

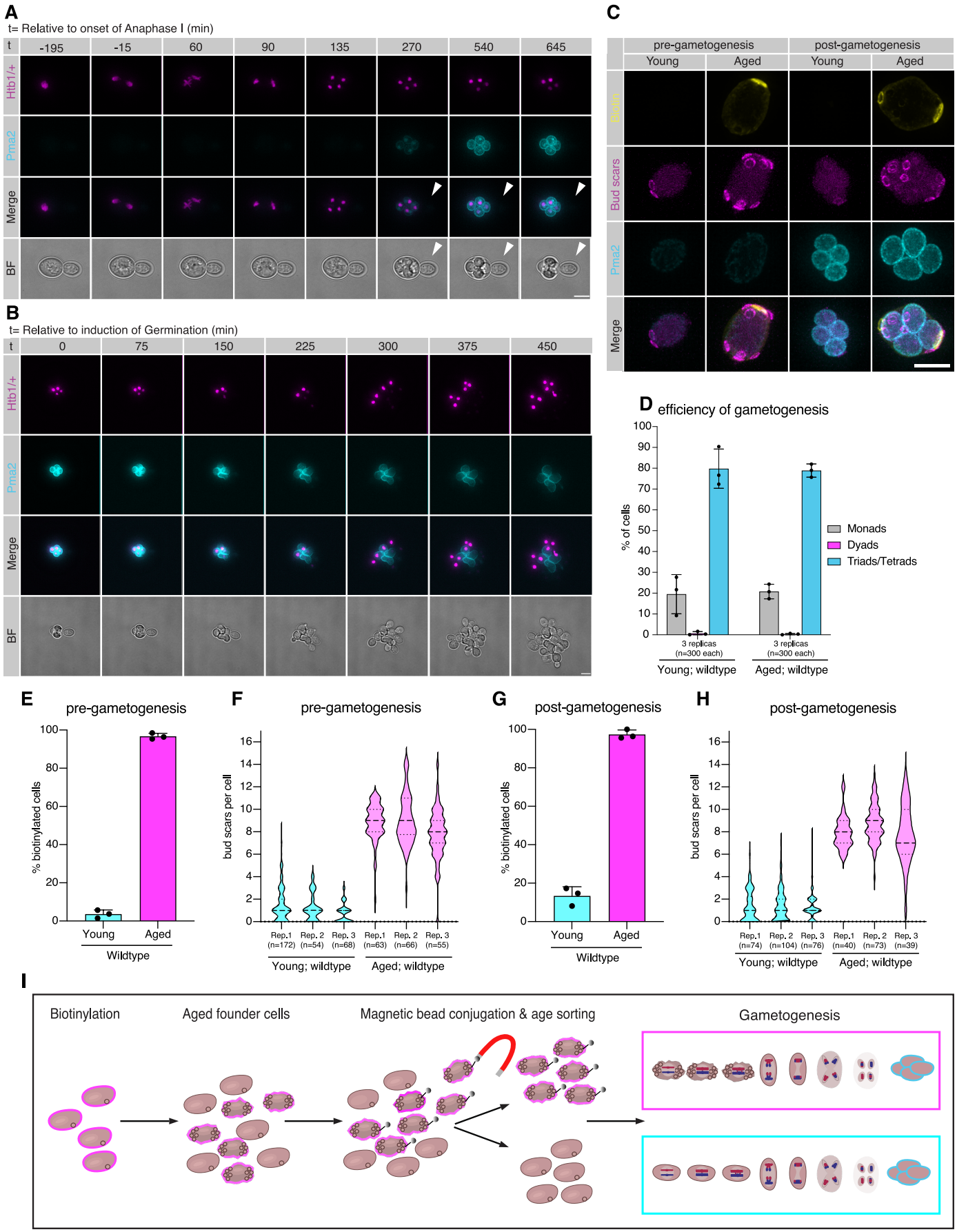
A
t= Relative to onset of Anaphase I (min)
t
-195
-15
60
90
135
270
540
645
Htb1/+
Pma2
Merge
BF
B
t= Relative to induction of Germination (min)
0
75
150
225
300
375
450
C
pre-gametogenesis
post-gametogenesis
Young
Aged
Biotin
Bud scars
D
efficiency of gametogenesis
% of cells
Monads
Dyads
Triads/Tetrads
3 replicas (n=300 each)
Young; wildtype
Aged; wildtype
E
pre-gametogenesis
% biotinylated cells
Young
Aged
Wildtype
F
pre-gametogenesis
bud scars per cell
Rep.1 (n=172)
Rep. 2 (n=54)
Rep. 3 (n=68)
Rep.1 (n=63)
Rep. 2 (n=66)
Rep. 3 (n=55)
G
post-gametogenesis
H
post-gametogenesis
Rep.1 (n=74)
Rep. 2 (n=104)
Rep. 3 (n=76)
Rep.1 (n=40)
Rep. 2 (n=73)
Rep. 3 (n=39)
I
Biotinylation
Aged founder cells
Magnetic bead conjugation & age sorting
Gametogenesis

Figure 2. Gametogenesis-specific expression of Pma2 remains detectable post-germination in age sorted gametes

(**A**) Montage of max-intensity projected diploid cell progressing through gametogenesis visualizing Pma2-GFP (cyan) and a Htb1-mCherry (magenta) marking histones. (**B**) Montage of a germinating max-intensity projected tetrad visualizing Pma2-GFP (cyan) and a Htb1-mCherry (magenta) marking histones. (**C**) Representative age sorted pre-gametogenic max-intensity projected cells (left panel) and post-gametogenic tetrads (right panel) visualizing biotin label (yellow), chitin rich bud scars (magenta) and Pma2-GFP (cyan). (**D**) Quantifying fraction of tetrads in young (79.8 ± 9.43%; mean ± SD, 3 replicas n=300 each) and aged (aged: 78.89 ± 3.17 %, mean ± SD, 3 replicas n=300 each) post gametogenic wildtype cell populations. (**E**) Quantifying fraction of biotinylated cells in young (3.63 ± 2.12 %, mean ± SD, 3 replicas, n=175, 54 and 68 respectively) and aged (96.74 ± 1.58 %, mean ± SD, 3 replicas, n=65, 66 and 55 respectively) wildtype cell populations. (**F**) Quantification of replicative age by assessing number of bud scars in young (1.16 ± 0.41, mean ± SD, n=3 replicas, n=172; 54 and 68 respectively) and aged (8.55 ± 0.66 (mean ± SD, 3 replicas, n=63, 66 and 55 respectively) wildtype cell populations. (**G**) Quantifying fraction of biotinylated tetrads in young (13.38 ± 4.74%, mean ± SD, n=3 replicas, n=74, 104 and 76 respectively) and aged (97.34 ± 2.33%, mean ± SD, 3 replicas, n=46, 73 and 39 respectively) wildtype populations after completion of gametogenesis. (**H**) Quantification of replicative age by assessing number of bud scars in young (1.31 ± 0.04, mean ± SD, 3 replicas, n=74, 104 and 76 respectively) and aged (8.17 ± 0.54, mean ± SD, 3 replicas, n=40, 73 and 39 respectively) wildtype gamete populations. (**I**) Schematic depiction of age sorting by biotin mediated magnetic bead conjugation. Scale bars are 5 µm and confidence intervals were calculated using the Wilson score method.

Figure 3

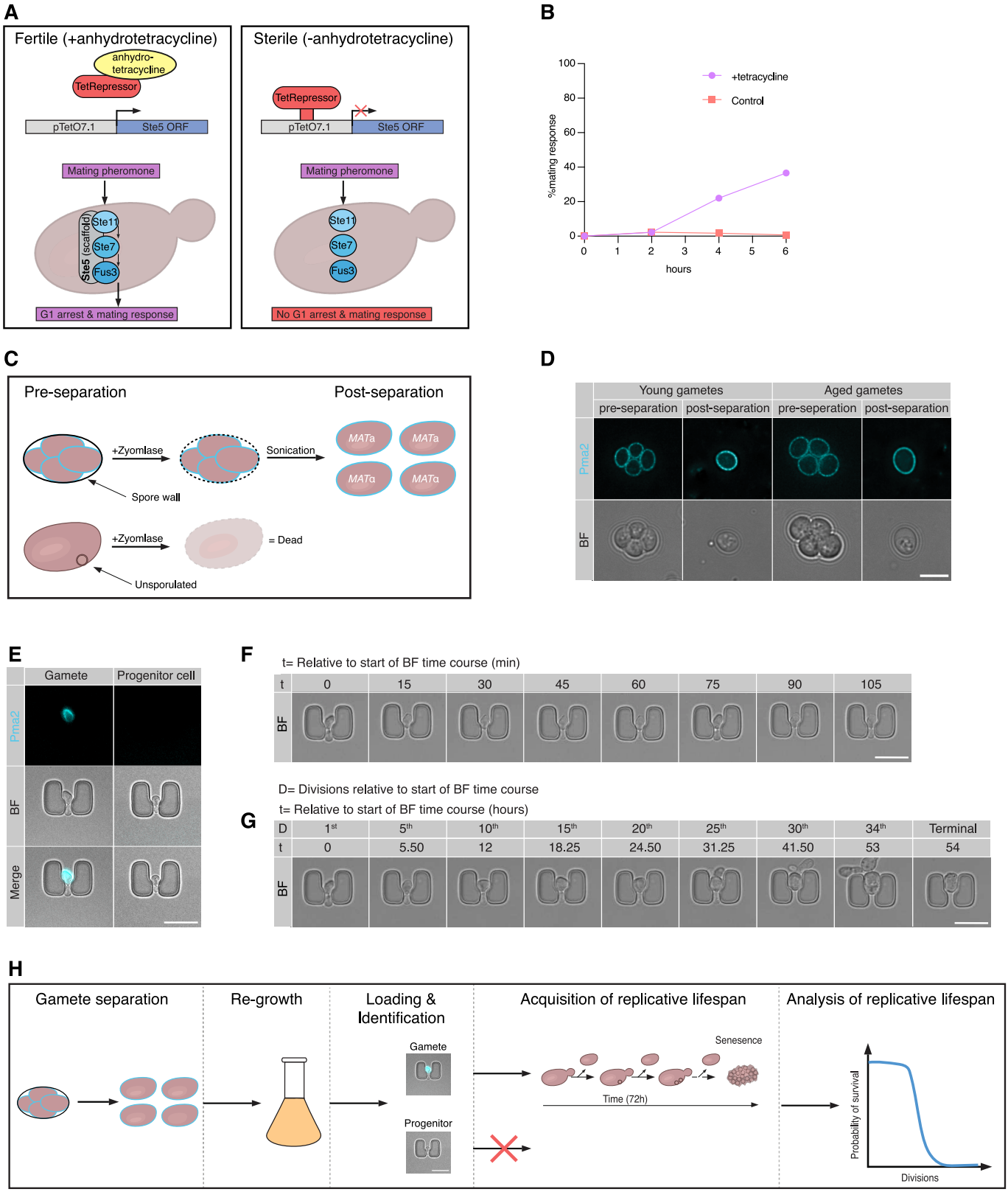
A
Fertile (+anhydrotetracycline)
anhydro-tetracycline
TetRepressor
pTetO7.1
Ste5 ORF
Mating pheromone
Ste5 (scaffold)
Ste11
Ste7
Fus3
G1 arrest & mating response
Sterile (-anhydrotetracycline)
TetRepressor
pTetO7.1
Ste5 ORF
Mating pheromone
Ste11
Ste7
Fus3
No G1 arrest & mating response
B
%mating response
hours
+tetracycline
Control
C
Pre-separation
Post-separation
+Zyomlase
Sonication
MATa
MATα
Spore wall
+Zyomlase
= Dead
Unsporulated
D
Young gametes
Aged gametes
pre-separation
post-separation
pre-seperation
post-separation
Pma2
BF
E
Gamete
Progenitor cell
Pma2
BF
Merge
F
t= Relative to start of BF time course (min)
t
0
15
30
45
60
75
90
105
BF
G
D= Divisions relative to start of BF time course
t= Relative to start of BF time course (hours)
D
1st
5th
10th
15th
20th
25th
30th
34th
Terminal
t
0
5.50
12
18.25
24.50
31.25
41.50
53
54
BF
H
Gamete separation
Re-growth
Loading & Identification
Acquisition of replicative lifespan
Analysis of replicative lifespan
Gamete
Progenitor
Senesence
Time (72h)
Probability of survival
Divisions

Figure 3. Separation of tetrads into single constitutive sterile gametes to assess gamete replicative lifespan using high-throughput microfluidics-based imaging devices
(**A**) Schematic depiction of genetic system to achieve constitutive sterility. (**B**) Quantification of mating response scoring hybrid formation upon 1:1 mixing of *MAT*a and *MAT*α cells. (**C**) Schematic depiction of tetrad separation procedure. (**D**) Representative single z-slices of pre- and post-separated young (left panel) and old (right panel) tetrads and gametes, respectively, visualizing brightfield and Pma2-GFP (cyan). (**E**) Representative Pma2-GFP positive gamete (left panel) and Pma2-GFP negative gamete progenitor (right panel) trapped in microfluidics-based devices visualizing brightfield and Pma2-GFP (cyan). (**F**) Representative gamete dividing twice over the time of two hours. (**G**) Same representative gamete as in (**F**) visualizing every 5th division until the terminal 34th division over the time of 54 hours. (**H**) Schematic depiction of the developed pipeline to assess gametes replicative lifespan. Scale bars are 5 µm.

Figure 4

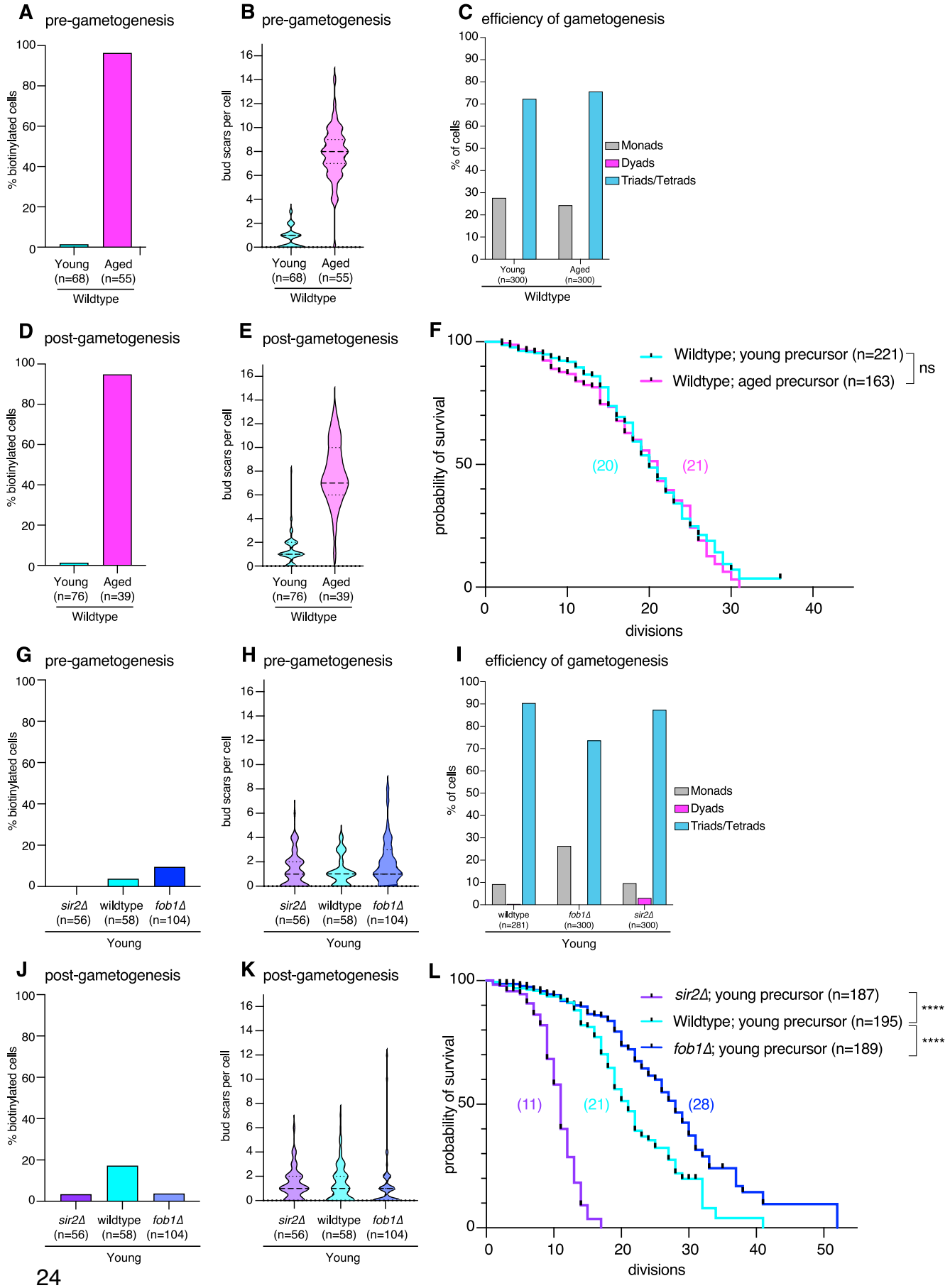
A pre-gametogenesis
% biotinylated cells
Young (n=68)
Aged (n=55)
Wildtype
B pre-gametogenesis
bud scars per cell
Young (n=68)
Aged (n=55)
Wildtype
C efficiency of gametogenesis
% of cells
Monads
Dyads
Triads/Tetrads
Young (n=300)
Aged (n=300)
Wildtype
D post-gametogenesis
% biotinylated cells
Young (n=76)
Aged (n=39)
Wildtype
E post-gametogenesis
bud scars per cell
Young (n=76)
Aged (n=39)
Wildtype
F
probability of survival
Wildtype; young precursor (n=221)
Wildtype; aged precursor (n=163)
ns
(20)
(21)
divisions
G pre-gametogenesis
% biotinylated cells
sir2Δ (n=56)
wildtype (n=58)
fob1Δ (n=104)
Young
H pre-gametogenesis
bud scars per cell
sir2Δ (n=56)
wildtype (n=58)
fob1Δ (n=104)
Young
I efficiency of gametogenesis
% of cells
Monads
Dyads
Triads/Tetrads
wildtype (n=281)
fob1Δ (n=300)
sir2Δ (n=300)
Young
J post-gametogenesis
% biotinylated cells
sir2Δ (n=56)
wildtype (n=58)
fob1Δ (n=104)
Young
K post-gametogenesis
bud scars per cell
sir2Δ (n=56)
wildtype (n=58)
fob1Δ (n=104)
Young
L
probability of survival
sir2Δ; young precursor (n=187)
Wildtype; young precursor (n=195)
fob1Δ; young precursor (n=189)
****
****
(11)
(21)
(28)
divisions

Figure 4. Wildtype gametes completely reset replicative lifespan during gametogenesis & rang of replicative lifespan in gametes from known longevity mutants.
(**A**) Quantifying fraction of biotinylated cells in young (1.5%, 95% CI: 0.3–7.9%, n=68) and aged (96.4%, 95% CI: 87.7–99.0%, n=55) wildtype cell populations. (**B**) Quantification of replicative age by assessing number of bud scars in young (0.72± 0.84, mean ± SD, n=68) and aged (7.8 ± 2.2, mean ± SD, n=55) wildtype cell populations. (**C**) Quantifying fraction of tetrads in young (72.3%, 95% CI: 67.0–77.1%, n=300) and aged (75.7%, 95% CI: 70.5–80.2% n=300) post gametogenic cell populations. (**D**) Quantifying fraction of biotinylated tetrads in young (1.3%, 95% CI: 0.2–7.1%, n=76) and aged (94.9%, 95% CI: 83.1–98.6%, n=39) wildtype populations after completion of gametogenesis. (**E**) Quantification of replicative age by assessing number of bud scars in young (1.3± 1.2, mean ± SD, n=76) and aged (7.8± 2.6, mean ± SD, n=39) wildtype gamete populations. (**F**) Quantification of replicative lifespan of young (median lifespan=20, n=221, 120 censored subjects, 1 technical replicate) and aged (median lifespan=21, n=163, 89 censored subjects, p=0.5058 compared to young, 1 technical replicate) wildtype gametes. Confidence intervals were calculated using the Wilson score method and statistical significance for differences between replicative lifespans was calculated using the Log-rank (Mantel-cox) test. (**G**) Quantifying fraction of biotinylated cells in young *sir2*Δ (none, n=78), wildtype (3.7%, 95% CI: 1–12.5%, n=54) and *fob1*Δ (9.5%, 95% CI: 3.8–22.1%, n=42) cell populations. (**H**) Quantification of replicative age by assessing number of bud scars in young *sir2*Δ (1.3± 1.4, mean ± SD, n=79), wildtype (1.2 ± 1.2, mean ± SD, n=54) and *fob1*Δ (1.9 ± 1.8, mean ± SD, n=42) cell populations. (**I**) Quantifying fraction of tetrads in young *sir2*Δ (87.3 %, 95% CI: 83.1– 90.6%, n=300), wildtype (90.4 %, 95% CI: 86.4% – 93.3%, n=281) and *fob1*Δ (73.7%, 95% CI: 68.4–78.3%, n=300) post gametogenic cell populations. (**J**) Quantifying fraction of biotinylated tetrads in young *sir2*Δ (3.4%, 95% CI: 1.0–11.7%, n=58), wildtype (17.3%, 95% CI: 11.2–25.7%, n=104) and *fob1*Δ (3.8%, 95% CI: 1.0–12.8%, n=53) populations after completion of gametogenesis. (**K**) Quantification of replicative age by assessing number of bud scars in young *sir2*Δ (1.3± 1.3, mean ± SD, n=56), wildtype (1.4± 1.5, mean ± SD, n=104) and *fob1*Δ (11.2± 2.2, mean ± SD, n=53) gamete populations. (**L**) Quantification of replicative lifespan of young *sir2*Δ (median lifespan=11, n=187, 80 censored subjects, p<0.0001 compared to wildtype), wildtype (median lifespan=21, n=195, 103 censored subjects) and *fob1*Δ (median lifespan=28, n=286, 174 censored subjects, p<0.0001 compared to wildtype) gametes.

Figure 5

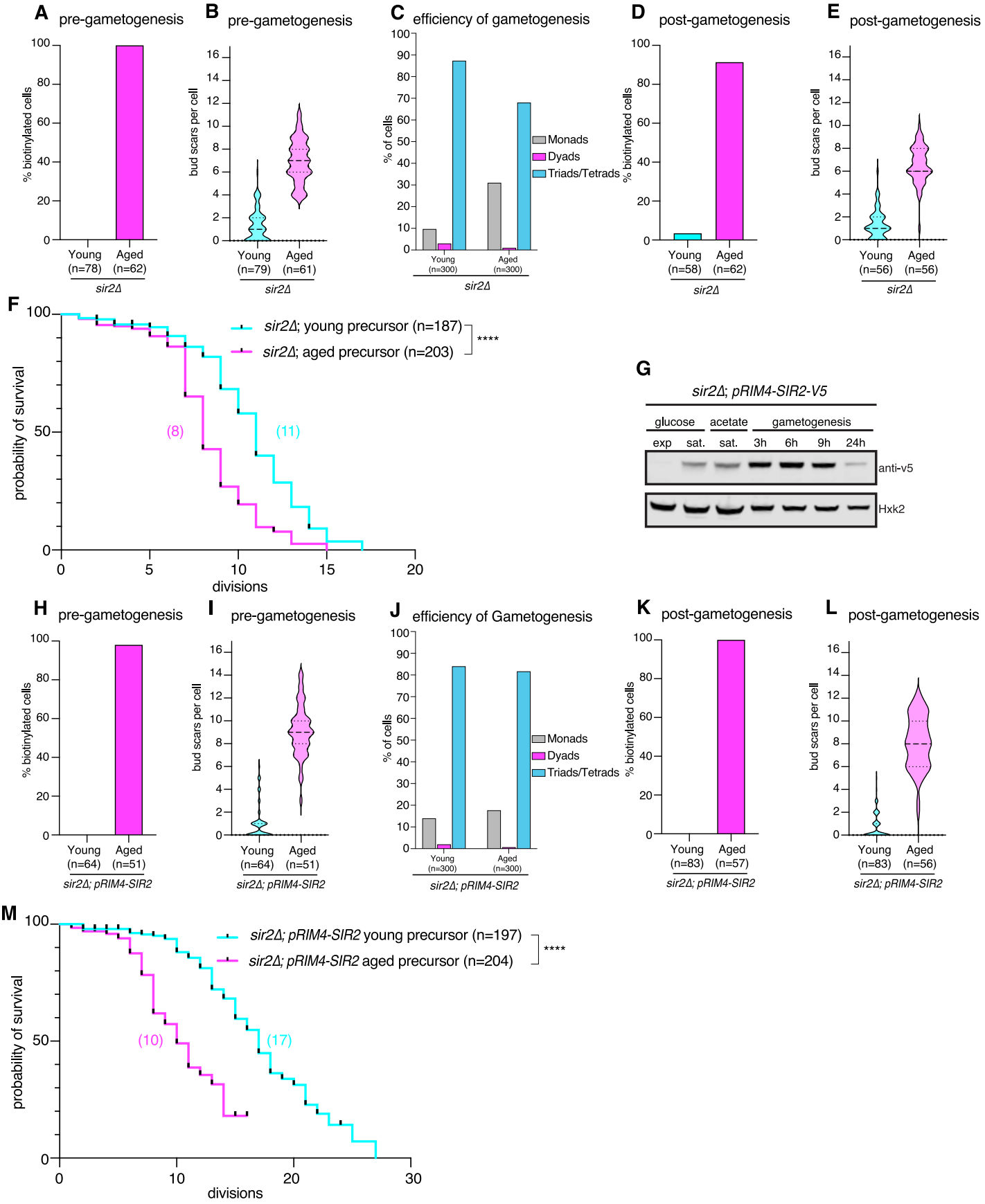
A pre-gametogenesis
% biotinylated cells
Young (n=78)
Aged (n=62)
sir2Δ
B pre-gametogenesis
bud scars per cell
Young (n=79)
Aged (n=61)
sir2Δ
C efficiency of gametogenesis
% of cells
Monads
Dyads
Triads/Tetrads
Young (n=300)
Aged (n=300)
sir2Δ
D post-gametogenesis
% biotinylated cells
Young (n=58)
Aged (n=62)
sir2Δ
E post-gametogenesis
bud scars per cell
Young (n=56)
Aged (n=56)
sir2Δ
F
probability of survival
sir2Δ; young precursor (n=187)
sir2Δ; aged precursor (n=203)
****
(8)
(11)
divisions
G
sir2Δ; pRIM4-SIR2-V5
glucose
acetate
gametogenesis
exp
sat.
sat.
3h
6h
9h
24h
anti-v5
Hxk2
H pre-gametogenesis
% biotinylated cells
Young (n=64)
Aged (n=51)
sir2Δ; pRIM4-SIR2
I pre-gametogenesis
bud scars per cell
Young (n=64)
Aged (n=51)
sir2Δ; pRIM4-SIR2
J efficiency of Gametogenesis
% of cells
Monads
Dyads
Triads/Tetrads
Young (n=300)
Aged (n=300)
sir2Δ; pRIM4-SIR2
K post-gametogenesis
% biotinylated cells
Young (n=83)
Aged (n=57)
sir2Δ; pRIM4-SIR2
L post-gametogenesis
bud scars per cell
Young (n=83)
Aged (n=56)
sir2Δ; pRIM4-SIR2
M
probability of survival
sir2Δ; pRIM4-SIR2 young precursor (n=197)
sir2Δ; pRIM4-SIR2 aged precursor (n=204)
****
(10)
(17)
divisions

Figure 5. *sir2*Δ mutants and gametogenesis specific Sir2 expression both fail to reset replicative lifespan of gametes

(**A**) Quantifying fraction of biotinylated cells in young (none, n=78, same data as shown in Fig. 4A) and aged (all, n=78) *sir2*Δ cell populations. (**B**) Quantification of replicative age by assessing number of bud scars in young (1.3± 1.4, mean ± SD, n=79, same data as shown in Fig. 4B) and aged (7± 1.9, mean ± SD, n=61) *sir2*Δ cell populations. (**C**) Quantifying fraction of tetrads in young (87.3% 95% CI: 83.1–90.6% n=300, same data as shown in Fig. 4E) and aged (68.0% (95% CI: 62.5–73.0%, n=300) post gametogenic *sir2*Δ cell populations. (**D**) Quantifying fraction of biotinylated tetrads in young (3.4%, 95% CI: 1.0–11.7%, n=58, same data as shown in Fig. 4C) and aged (91.9%, 95% CI: 82.5–96.5%, n=62) *sir2*Δ populations after completion of gametogenesis. (**E**) Quantification of replicative age by assessing number of bud scars in young (1.3± 1.3, mean ± SD, n=56, same data as shown in Fig. 4D) and aged (6.6± 1.6, mean ± SD, n=56) *sir2*Δ gamete populations. (**F**) Quantification of replicative lifespan of young (median lifespan=11, n=187, 80 censored subjects, same data as shown in Fig. 3F) and aged *sir2*Δ (median lifespan=8, n=203, 103 censored subjects, p<0.0001 compared to young) gametes. (**G**) Immunoblot to quantify pRim4-Sir2 levels (anti-V5) and loading control (Hxk2) in growth media containing ether 2% glucose (glucose) or acetate (acetate) and at different timepoints upon transfer to gametogenesis-inducing media (gametogenesis). (**H**) Quantifying fraction of biotinylated cells in young (none, n=64) and aged (98.0%, 95% CI: 89.7–99.7%, n=51) *pRIM4-SIR2 sir2*Δ cell populations. (**I**) Quantification of replicative age by assessing number of bud scars in young (0.98± 1.5, mean ± SD, n=64) and aged (9.1± 2.2 (mean ± SD, n=51) *pRIM4-SIR2 sir2*Δ cell populations. (**J**) Quantifying fraction of tetrads in young (84 %, 95% CI: 79.4–87.7%, n=300) and aged (81.7%, 95% CI: 76.9–85.6%, n=300) post gametogenic *pRIM4-SIR2 sir2*Δ cell populations. (**K**) Quantifying fraction of biotinylated tetrads in young (none, n=83) and aged (all, n=57) *pRIM4-SIR2 sir2*Δ populations after completion of gametogenesis. (**L**) Quantification of replicative age by assessing number of bud scars in young (0.72± 1.1, mean ± SD, n=83) and aged 8.1± 2.3 (mean ± SD, n=56) *pRIM4-SIR2 sir2*Δ gamete populations. (**M**) Quantification of replicative lifespan of young (median lifespan17, n=197, 129 censored subjects, 1 technical replicate) and aged *pRIM4-SIR2 sir2*Δ (median lifespan=10 (n=204, 139 censored subjects, p<0.0001 compared to young, 1 technical replicate) gametes. Confidence intervals were calculated using the Wilson score method and statistical significance for differences between replicative lifespans was calculated using the Log-rank (Mantel-cox) test.

Figure 6

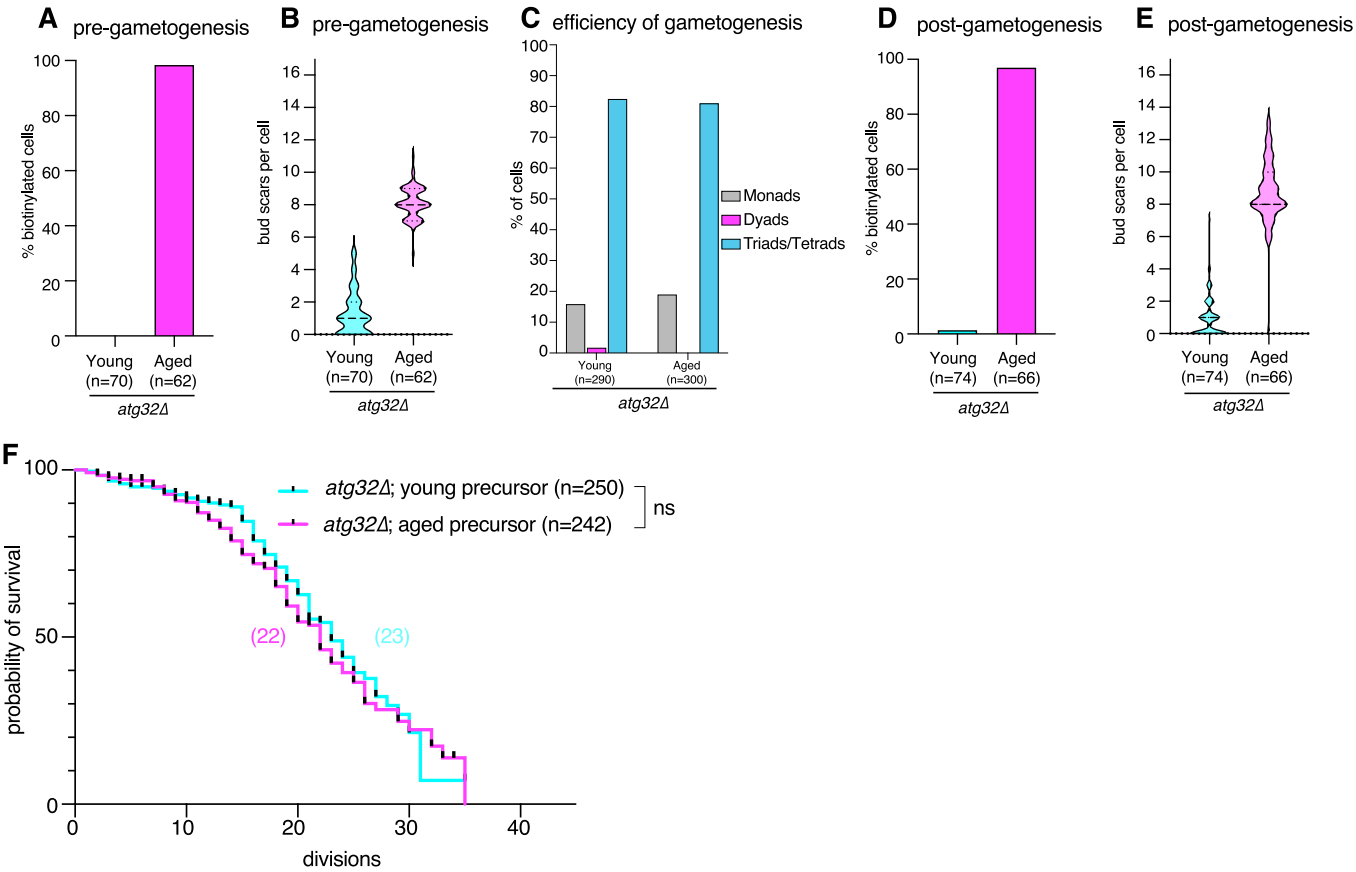

Figure 6. *atg32*Δ mutants completely reset replicative lifespan of gametes
(**A**) Quantifying fraction of biotinylated cells in young (none, n=70) and aged (98.4%, 95% CI: 91.4–99.7%, n=62) *atg32*Δ cell populations. (**B**) Quantification of replicative age by assessing number of bud scars in young (1.3± 1.4, mean ± SD, n=70) and aged (8.1± 0.98, mean ± SD, n=62) *atg32*Δ cell populations. (**C**) Quantifying fraction of tetrads in young (82.4%, 95% CI: 77.6–86.4%), n=290) and aged (81.0%, 95% CI: 76.2–85.0%, n=300) post-gametogenic *atg32*Δ cell populations. (**D**) Quantifying fraction of biotinylated tetrads in young (1.4%, 95% CI: 0.2–7.3%, n=74) and aged 97.0% (95% CI: 89.6–99.2%, n=66) *atg32*Δ populations after completion of gametogenesis. (**E**) Quantification of replicative age by assessing number of bud scars in young (0.93± 1.3, mean ± SD, n=74) and aged (8.7± 2, mean ± SD, n=66) *atg32*Δ gamete populations. (**F**) Quantification of replicative lifespan of young (median lifespan=23, n=242, 151 censored subjects, 1 technical replicate) and aged (median lifespan=22, n=250, 151 censored subjects, p=0.2691) *atg32*Δ gametes. Confidence intervals were calculated using the Wilson score method and statistical significance for differences between replicative lifespans was calculated using the Log-rank (Mantel-cox) test.

Figure 7

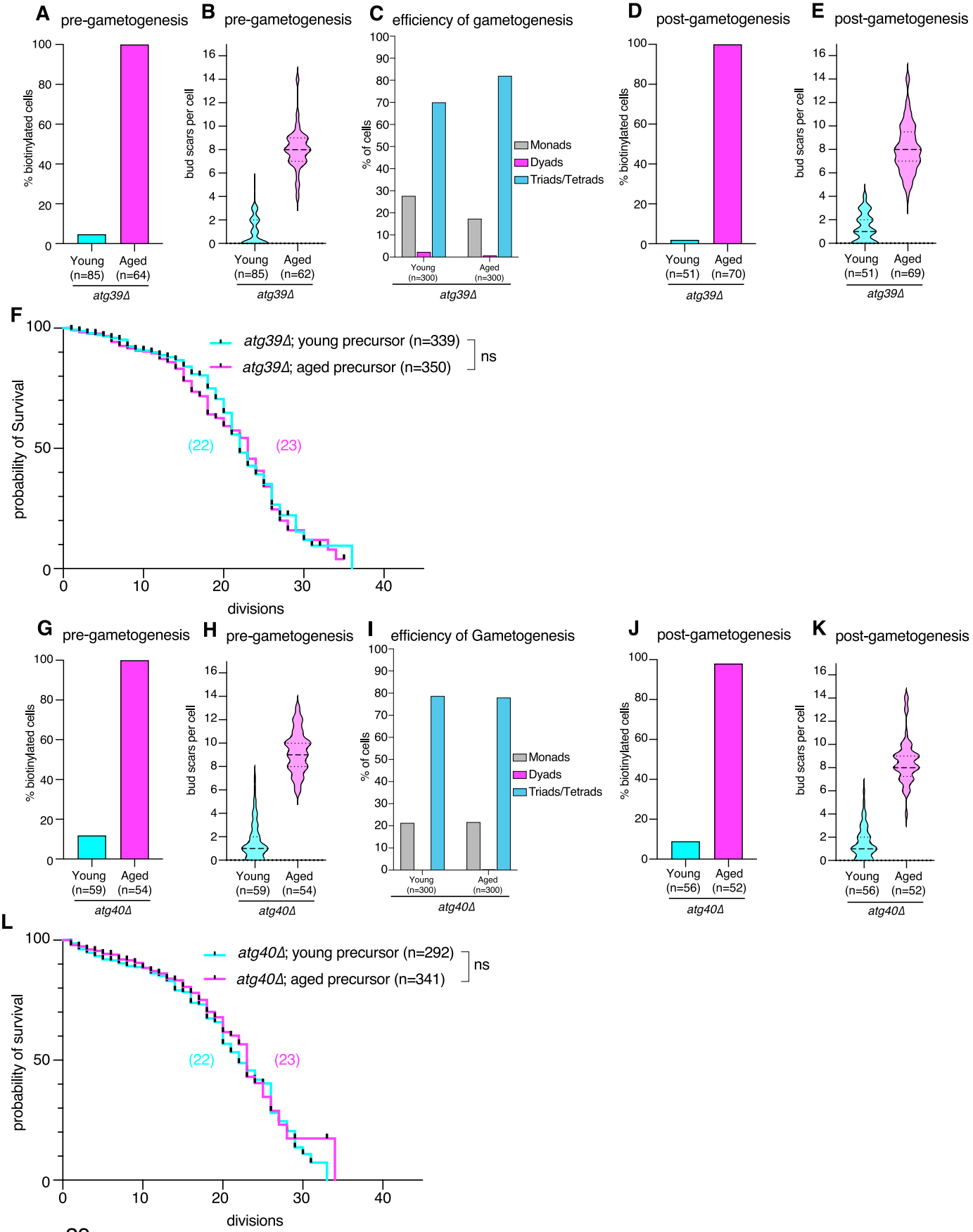
A pre-gametogenesis
% biotinylated cells
Young (n=85)
Aged (n=64)
atg39Δ
B pre-gametogenesis
bud scars per cell
Young (n=85)
Aged (n=62)
atg39Δ
C efficiency of gametogenesis
% of cells
Monads
Dyads
Triads/Tetrads
Young (n=300)
Aged (n=300)
atg39Δ
D post-gametogenesis
% biotinylated cells
Young (n=51)
Aged (n=70)
atg39Δ
E post-gametogenesis
bud scars per cell
Young (n=51)
Aged (n=69)
atg39Δ
F
probability of Survival
atg39Δ; young precursor (n=339)
atg39Δ; aged precursor (n=350)
ns
(22)
(23)
divisions
G pre-gametogenesis
% biotinylated cells
Young (n=59)
Aged (n=54)
atg40Δ
H pre-gametogenesis
bud scars per cell
Young (n=59)
Aged (n=54)
atg40Δ
I efficiency of Gametogenesis
% of cells
Monads
Dyads
Triads/Tetrads
Young (n=300)
Aged (n=300)
atg40Δ
J post-gametogenesis
% biotinylated cells
Young (n=56)
Aged (n=52)
atg40Δ
K post-gametogenesis
bud scars per cell
Young (n=56)
Aged (n=52)
atg40Δ
L
probability of survival
atg40Δ; young precursor (n=292)
atg40Δ; aged precursor (n=341)
ns
(22)
(23)
divisions

Figure 7. *atg39*Δ and *atg40*Δ single mutants completely reset replicative lifespan of gametes

(**A**) Quantifying fraction of biotinylated cells in young (3.5%, 95% CI: 1.2–9.9%, n=85) and aged (all, n=64) *atg39*Δ cell populations. (**B**) Quantification of replicative age by assessing number of bud scars in young (0.98± 1.2, mean ± SD, n=85) and aged (8.1± 1.8, mean ± SD, n=64) *atg39*Δ cell populations. (**C**) Quantifying fraction of tetrads in young (70.0%, 95% CI: 64.6–74.9%, n=300) and aged (82.0% (95% CI: 77.3–85.9%, n=300) post gametogenic *atg39*Δ cell populations. (**D**) Quantifying fraction of biotinylated tetrads in young (2.0%, 95% CI: 0.3–10.3%, n=51) and aged (all, n=69) *atg39*Δ populations after completion of gametogenesis. (**E**) Quantification of replicative age by assessing number of bud scars in young (1.3± 1.2, mean ± SD, n=51) and aged (8.1 ± 2.1, mean ± SD, n=69) *atg39*Δ gamete populations. (**F**) Quantification of replicative lifespan of young (median lifespan=22, n=339, 188 censored subjects) and aged *atg32*Δ (median lifespan=23, n=350, 225 censored subjects, p=0.418 compared to young) gametes. (**G**) Quantifying fraction of biotinylated cells in young (11.9%, 95% CI: 5.9–22.5%, n=59) and aged (all, n=54) *atg40*Δ cell populations. (**H**) Quantification of replicative age by assessing number of bud scars in young (1.6± 1.6, mean ± SD, n=59) and aged (9.3± 1.8, mean ± SD, n=54) *atg40*Δ cell populations. (**I**) Quantifying fraction of tetrads in young (78.7%, 95% CI: 73.7–82.9%, n=300) and aged (78.0%, 95% CI: 73.0–82.3%, n=300) post gametogenic *atg39*Δ cell populations. (**J**) Quantifying fraction of biotinylated tetrads in young (8.9%, 95% CI: 3.9–19.3%) and aged (98.1%, 95% CI: 89.9–99.7%, n=52) *atg40*Δ populations after completion of gametogenesis. (**K**) Quantification of replicative age by assessing number of bud scars in young (1.4± 1.4, mean ± SD, n=56), and aged (8.6± 1.9, mean ± SD, n=52) *atg40*Δ gamete populations. (**L**) Quantification of replicative lifespan of young (median lifespan=22, n=292, 176 censored subjects) and aged *atg32*Δ (median lifespan=23, n=341, 256 censored subjects, p=0.389 compared to young) gametes. Confidence intervals were calculated using the Wilson score method and statistical significance for differences between replicative lifespans was calculated using the Log-rank (Mantel-cox) test.

Figure 8

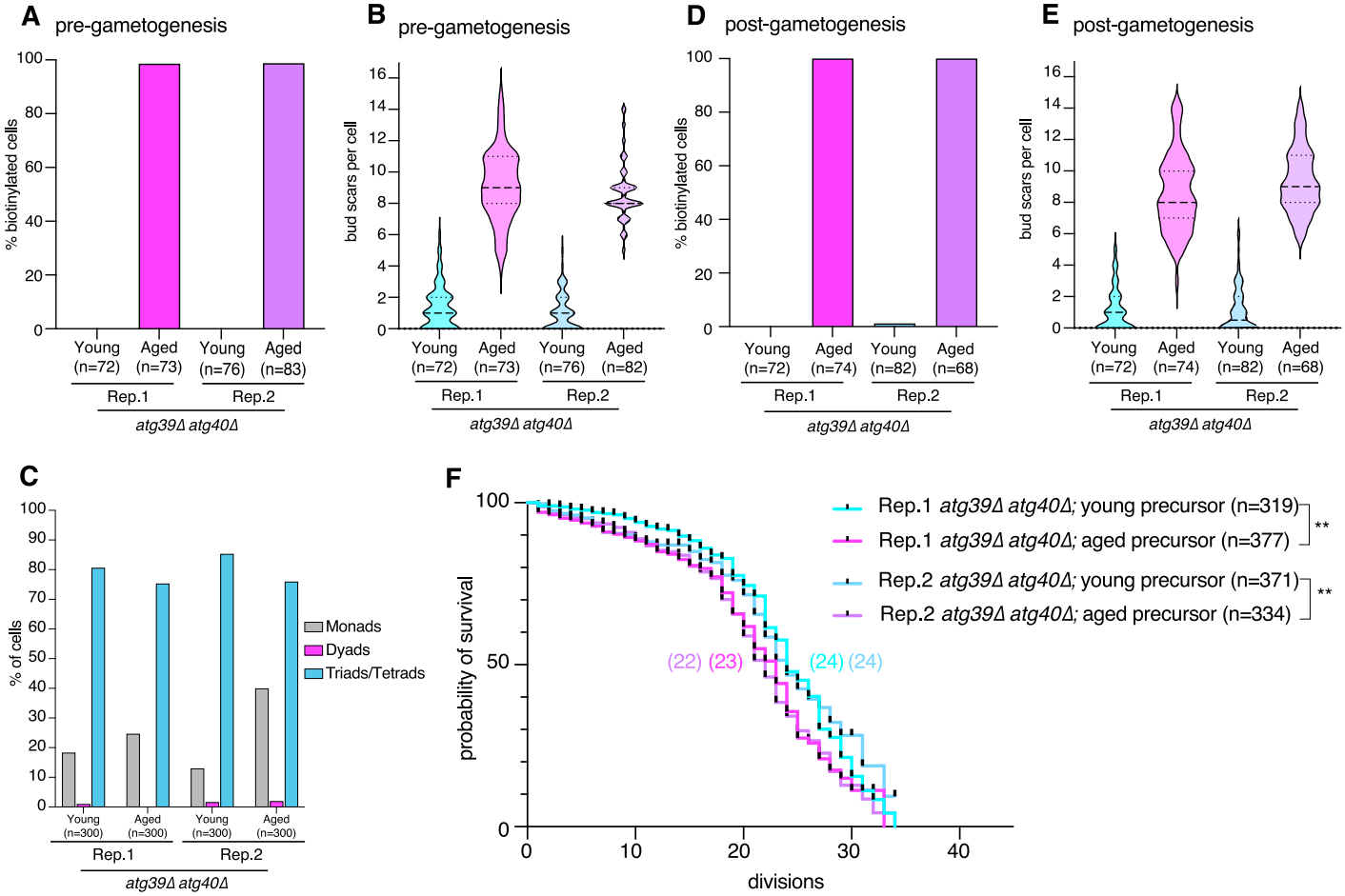
A pre-gametogenesis
% biotinylated cells
Young (n=72)
Aged (n=73)
Young (n=76)
Aged (n=83)
Rep.1
Rep.2
atg39Δ atg40Δ
B pre-gametogenesis
bud scars per cell
Young (n=72)
Aged (n=73)
Young (n=76)
Aged (n=82)
Rep.1
Rep.2
atg39Δ atg40Δ
D post-gametogenesis
% biotinylated cells
Young (n=72)
Aged (n=74)
Young (n=82)
Aged (n=68)
Rep.1
Rep.2
atg39Δ atg40Δ
E post-gametogenesis
bud scars per cell
Young (n=72)
Aged (n=74)
Young (n=82)
Aged (n=68)
Rep.1
Rep.2
atg39Δ atg40Δ
C
% of cells
Monads
Dyads
Triads/Tetrads
Young (n=300)
Aged (n=300)
Young (n=300)
Aged (n=300)
Rep.1
Rep.2
atg39Δ atg40Δ
F
probability of survival
divisions
Rep.1 atg39Δ atg40Δ; young precursor (n=319)
Rep.1 atg39Δ atg40Δ; aged precursor (n=377)
Rep.2 atg39Δ atg40Δ; young precursor (n=371)
Rep.2 atg39Δ atg40Δ; aged precursor (n=334)
**
**
(22) (23)
(24) (24)

Figure 8. *atg39*Δ *atg40*Δ double mutants fail to reset replicative lifespan during gametogenesis

(**A**) Quantifying fraction of biotinylated cells in *atg39*Δ *atg40*Δ cell populations: Replicate 1 (Rep. 1) young (none, n=72) and aged (98.6%, 95% CI: 92.6–99.8%, n=73); Replicate 2 (Rep. 2) young (none, n=76) and aged (98.8%, 95% CI: 93.5–99.8%, n=83). (**B**) Quantification of replicative age by assessing number of bud scars in *atg39*Δ *atg40*Δ cell populations: Rep. 1 young (1.4± 1.4, mean ± SD, n=72) and aged (9.1± 2.3, mean ± SD, n=73); Rep. 2 young (1 ± 1.2, mean ± SD, n=76) and aged (8.7± 1.9, mean ± SD, n=82). (**C**) Quantifying fraction of tetrads in post gametogenic *atg39*Δ *atg40*Δ cell populations: Rep.1 young (80.7%, 95% CI: 75.8–84.7%, n=300) and aged (75.3%, 95% CI: 70.2–79.9%, n=300); Rep. 2 young (85.3%, 95% CI: 80.9–88.9%, n=300) and aged (76.0%, 95% CI: 70.9–80.5%, n=300). (**D**) Quantifying fraction of biotinylated tetrads in *atg39*Δ *atg40*Δ populations after completion of gametogenesis: Rep.1 young (none, n=72) and aged (all, n=74); Rep. 2 young (1.2%, 95% CI: 0.2–6.6%, n=82) and aged (all, n=68). (**E**) Quantification of replicative age by assessing number of bud scars in *atg39*Δ *atg40*Δ tetrad populations: Rep. 1 young (1.1± 1.4, mean ± SD, n=72) and aged of (8.6± 2.5, mean ± SD, n=74); Rep. 2 young (1.1± 1.5, mean ± SD, n=82) and aged of (9.4± 2, mean ± SD, n=68) (**F**) Quantification of replicative lifespan of *atg39*Δ *atg40*Δ gametes: Rep.1 young (median lifespan=24, n=319, 195 censored subjects) and aged (median lifespan=23, n=377, 238 censored subjects, p=0.0017 compared to young); Rep. 2 young (median lifespan=24, n=371, 240 censored subjects) and aged (median lifespan=22, n=334, 219 censored subjects, p=0.0080 compared to young). Confidence intervals were calculated using the Wilson score method and statistical significance for differences between replicative lifespans was calculated using the Log-rank (Mantel-cox) test.

Figure S1

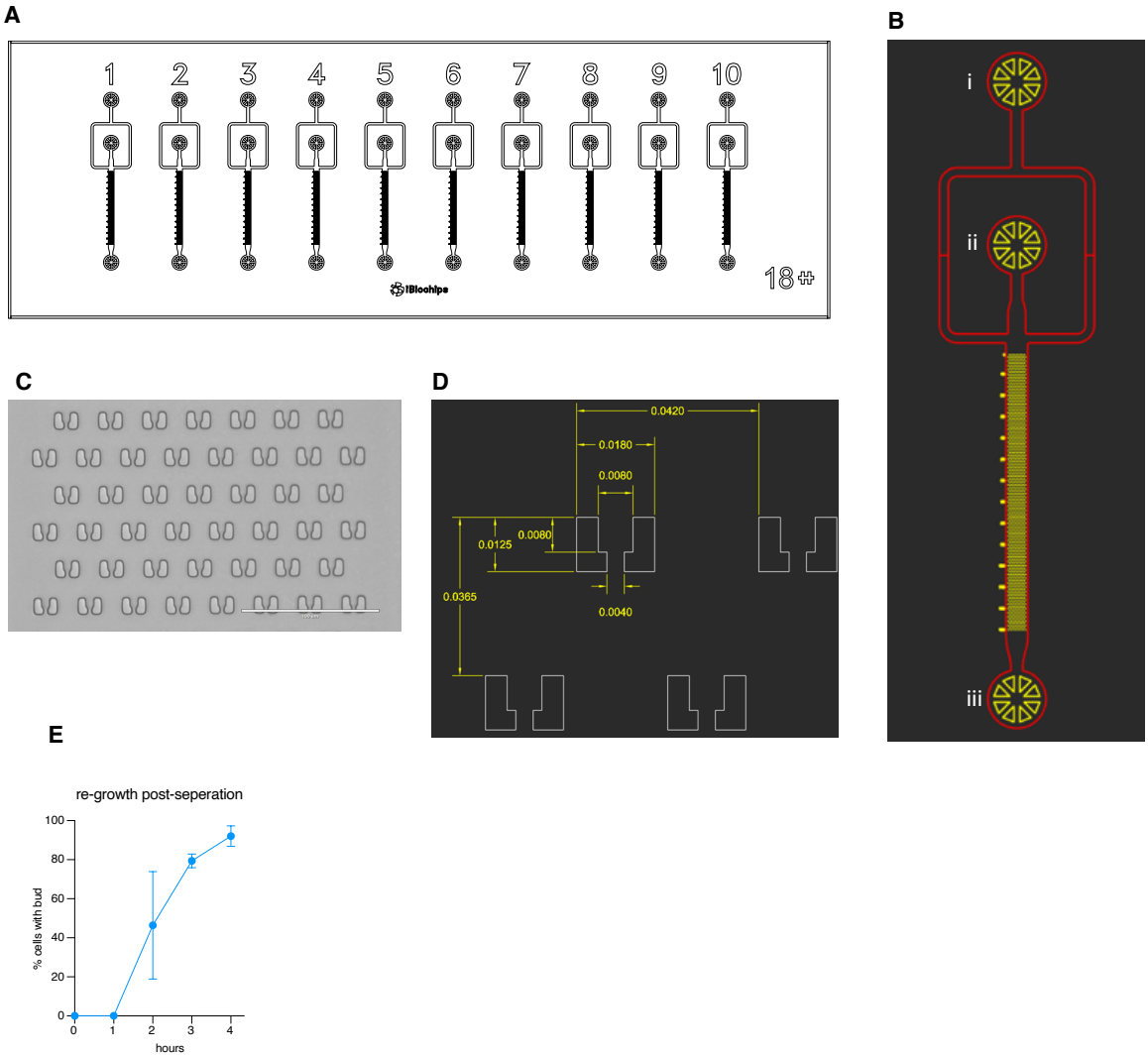

Fig S1. Custom-built U-trap microfluidic devices with specific dimensions for vegetatively growing haploid SK1 cells.

(**A**) Schematic view of one microfluidic device with 10 separate imaging units. (**B**) Schematic overview of one unit with (i) media inlet; cell loading inlet (ii) and waste outlet (iii). During the experiment media flows from media inlet (i) to waste outlet (iii) while cell loading inlet is plugged with a solid stainless-steel pin. (**C**) Image of U-traps and spacing in one unit, scale bar is 100 µm. (**D**) Custom developed SK1 specific dimensions of trap width and height (8 µm), exit channel width (4 µm), and spacing between traps (24 µm). (**E**) Monitoring of re-growth of separated gametes in glucose containing liquid culture by scoring emergence of buds.

References

Bellí, G., Garí, E., Piedrafita, L., Aldea, M., Herrero, E., 1998. An activator/repressor dual system allows tight tetracycline-regulated gene expression in budding yeast. Nucleic Acids Res 26, 942–947. https://doi.org/10.1093/nar/26.4.942

Brar, G.A., Yassour, M., Friedman, N., Regev, A., Ingolia, N.T., Weissman, J.S., 2012. High-Resolution View of the Yeast Meiotic Program Revealed by Ribosome Profiling. Science 335, 552–557. https://doi.org/10.1126/science.1215110

Cabib, E., Bowers, B., 1971. Chitin and Yeast Budding: LOCALIZATION OF CHITIN IN YEAST BUD SCARS. Journal of Biological Chemistry 246, 152–159. https://doi.org/10.1016/S0021-9258(18)62543-8

Carmelo, V., Santos, H., Sá-Correia, I., 1997. Effect of extracellular acidification on the activity of plasma membrane ATPase and on the cytosolic and vacuolar pH of Saccharomyces cerevisiae. Biochim Biophys Acta 1325, 63–70. https://doi.org/10.1016/s0005-2736(96)00245-3

Chen, K.L., Crane, M.M., Kaeberlein, M., 2017. Microfluidic Technologies for Yeast Replicative Lifespan Studies. Mech Ageing Dev 161, 262–269. https://doi.org/10.1016/j.mad.2016.03.009

Cheng, Z., Otto, G.M., Powers, E.N., Keskin, A., Mertins, P., Carr, S.A., Jovanovic, M., Brar, G.A., 2018. Pervasive, Coordinated Protein-Level Changes Driven by Transcript Isoform Switching during Meiosis. Cell 172, 910-923.e16. https://doi.org/10.1016/j.cell.2018.01.035

Chol, K.-Y., Satterberg, B., Lyons, D.M., Elion, E.A., 1994. Ste5 tethers multiple protein kinases in the MAP kinase cascade required for mating in S. cerevisiae. Cell 78, 499–512. https://doi.org/10.1016/0092-8674(94)90427-8

Defossez, P.-A., Prusty, R., Kaeberlein, M., Lin, S.-J., Ferrigno, P., Silver, P.A., Keil, R.L., Guarente, L., 1999. Elimination of Replication Block Protein Fob1 Extends the Life Span of Yeast Mother Cells. Molecular Cell 3, 447–455. https://doi.org/10.1016/S1097-2765(00)80472-4

Deng, C., Saunders, W., 2001. RIM4 encodes a meiotic activator required for early events of meiosis in Saccharomyces cerevisiae. Mol Gen Genomics 266, 497–504. https://doi.org/10.1007/s004380100571

Denoth Lippuner, A., Julou, T., Barral, Y., 2014. Budding yeast as a model organism to study the effects of age. FEMS Microbiol Rev 38, 300–325. https://doi.org/10.1111/1574-6976.12060

Fang, O., Hu, X., Wang, L., Jiang, N., Yang, J., Li, B., Luo, Z., 2018. Amn1 governs post-mitotic cell separation in Saccharomyces cerevisiae. PLOS Genetics 14, e1007691. https://doi.org/10.1371/journal.pgen.1007691

Fernandes, A.R., Sá-Correia, I., 2003. Transcription patterns of PMA1 and PMA2 genes and activity of plasma membrane H+-ATPase in Saccharomyces cerevisiae during diauxic growth and stationary phase. Yeast 20, 207–219. https://doi.org/10.1002/yea.957

Foss, E.J., Lao, U., Dalrymple, E., Adrianse, R.L., Loe, T., Bedalov, A., 2017. SIR2 suppresses replication gaps and genome instability by balancing replication between repetitive and unique sequences. Proc Natl Acad Sci U S A 114, 552–557. https://doi.org/10.1073/pnas.1614781114

Gao, Z., Xu, J., Chen, K., Wang, S., Ouyang, Q., Luo, C., 2020. Comparative Analysis of Yeast Replicative Lifespan in Different Trapping Structures Using an Integrated Microfluidic System. Advanced Materials Technologies 5, 2000655. https://doi.org/10.1002/admt.202000655

Gibson, D.G., Young, L., Chuang, R.-Y., Venter, J.C., Hutchison, C.A., Smith, H.O., 2009. Enzymatic assembly of DNA molecules up to several hundred kilobases. Nat Methods 6, 343–345. https://doi.org/10.1038/nmeth.1318

Gladyshev, V.N., 2021. The Ground Zero of Organismal Life and Aging. Trends in Molecular Medicine 27, 11–19. https://doi.org/10.1016/j.molmed.2020.08.012

Hansen, M., Rubinsztein, D.C., Walker, D.W., 2018. Autophagy as a promoter of longevity: insights from model organisms. Nat Rev Mol Cell Biol 19, 579–593. https://doi.org/10.1038/s41580-018-0033-y

Higuchi-Sanabria, R., Pernice, W.M.A., Vevea, J.D., Alessi Wolken, D.M., Boldogh, I.R., Pon, L.A., 2014. Role of asymmetric cell division in lifespan control in Saccharomyces cerevisiae. FEMS Yeast Res 14, 1133–1146. https://doi.org/10.1111/1567-1364.12216

Hoggard, T.A., Chang, F., Perry, K.R., Subramanian, S., Kenworthy, J., Chueng, J., Shor, E., Hyland, E.M., Boeke, J.D., Weinreich, M., Fox, C.A., 2018. Yeast heterochromatin regulators Sir2 and Sir3 act directly at euchromatic DNA replication origins. PLOS Genetics 14, e1007418. https://doi.org/10.1371/journal.pgen.1007418

Hotz, M., Thayer, N.H., Hendrickson, D.G., Schinski, E.L., Xu, J., Gottschling, D.E., 2022. rDNA array length is a major determinant of replicative lifespan in budding yeast. Proceedings of the National Academy of Sciences 119, e2119593119. https://doi.org/10.1073/pnas.2119593119

Hughes, A.L., Gottschling, D.E., 2012. An early age increase in vacuolar pH limits mitochondrial function and lifespan in yeast. Nature 492, 261–265. https://doi.org/10.1038/nature11654

Ide, S., Miyazaki, T., Maki, H., Kobayashi, T., 2010. Abundance of Ribosomal RNA Gene Copies Maintains Genome Integrity. Science 327, 693–696. https://doi.org/10.1126/science.1179044

Jin, M., Li, Y., O'Laughlin, R., Bittihn, P., Pillus, L., Tsimring, L.S., Hasty, J., Hao, N., 2019. Divergent Aging of Isogenic Yeast Cells Revealed through Single-Cell Phenotypic Dynamics. Cell Systems 8, 242-253.e3. https://doi.org/10.1016/j.cels.2019.02.002

Jo, M.C., Liu, W., Gu, L., Dang, W., Qin, L., 2015. High-throughput analysis of yeast replicative aging using a microfluidic system. Proceedings of the National Academy of Sciences 112, 9364–9369. https://doi.org/10.1073/pnas.1510328112

Jones, D.L., 2007. Aging and the Germ Line: Where Mortality and Immortality Meet. Stem Cell Rev 3, 192–200. https://doi.org/10.1007/s12015-007-0009-3

Kaeberlein, M., Kirkland, K.T., Fields, S., Kennedy, B.K., 2004. Sir2-Independent Life Span Extension by Calorie Restriction in Yeast. PLoS Biol 2, e296. https://doi.org/10.1371/journal.pbio.0020296

Kaeberlein, M., McVey, M., Guarente, L., 1999. The SIR2/3/4 complex and SIR2 alone promote longevity in Saccharomyces cerevisiae by two different mechanisms. Genes Dev 13, 2570–2580. https://doi.org/10.1101/gad.13.19.2570

Kane, S.M., Roth, R., 1974. Carbohydrate Metabolism During Ascospore Development in Yeast. Journal of Bacteriology 118, 8–14. https://doi.org/10.1128/jb.118.1.8-14.1974

Kanki, T., Wang, K., Baba, M., Bartholomew, C.R., Lynch-Day, M.A., Du, Z., Geng, J., Mao, K., Yang, Z., Yen, W.-L., Klionsky, D.J., 2009a. A genomic screen for yeast mutants defective in selective mitochondria autophagy. Mol Biol Cell 20, 4730–4738. https://doi.org/10.1091/mbc.e09-03-0225

Kanki, T., Wang, K., Cao, Y., Baba, M., Klionsky, D.J., 2009b. Atg32 Is a Mitochondrial Protein that Confers Selectivity during Mitophagy. Developmental Cell 17, 98–109. https://doi.org/10.1016/j.devcel.2009.06.014

King, G.A., Goodman, J.S., Schick, J.G., Chetlapalli, K., Jorgens, D.M., McDonald, K.L., Ünal, E., 2019. Meiotic cellular rejuvenation is coupled to nuclear remodeling in budding yeast. eLife 8, e47156. https://doi.org/10.7554/eLife.47156

Kobayashi, O., Suda, H., Ohtani, T., Sone, H., 1996. Molecular cloning and analysis of the dominant flocculation geneFLO8 fromSaccharomyces cerevisiae. Molec. Gen. Genet. 251, 707–715. https://doi.org/10.1007/BF02174120

Kobayashi, T., Ganley, A.R.D., 2005. Recombination Regulation by Transcription-Induced Cohesin Dissociation in rDNA Repeats. Science 309, 1581–1584. https://doi.org/10.1126/science.1116102

Kobayashi, T., Horiuchi, T., Tongaonkar, P., Vu, L., Nomura, M., 2004. *SIR2* Regulates Recombination between Different rDNA Repeats, but Not Recombination within Individual rRNA Genes in Yeast. Cell 117, 441–453. https://doi.org/10.1016/S0092-8674(04)00414-3

Kondo-Okamoto, N., Noda, N.N., Suzuki, S.W., Nakatogawa, H., Takahashi, I., Matsunami, M., Hashimoto, A., Inagaki, F., Ohsumi, Y., Okamoto, K., 2012. Autophagy-related Protein 32 Acts as Autophagic Degron and Directly Initiates Mitophagy*. Journal of Biological Chemistry 287, 10631–10638. https://doi.org/10.1074/jbc.M111.299917

Lee, I.H., Cao, L., Mostoslavsky, R., Lombard, D.B., Liu, J., Bruns, N.E., Tsokos, M., Alt, F.W., Finkel, T., 2008. A role for the NAD-dependent deacetylase Sirt1 in the regulation of autophagy. Proceedings of the National Academy of Sciences 105, 3374–3379. https://doi.org/10.1073/pnas.0712145105

Lee, I.H., Yun, J., Finkel, T., 2013. The Emerging Links Between Sirtuins and Autophagy. Methods Mol Biol 1077, 259–271. https://doi.org/10.1007/978-1-62703-637-5_17

Lee, M.B., Dowsett, I.T., Carr, D.T., Wasko, B.M., Stanton, S.G., Chung, M.S., Ghodsian, N., Bode, A., Kiflezghi, M.G., Uppal, P.A., Grayden, K.A., Elala, Y.C., Tang, T.T., Tran, N.H.B., Tran, T.H.B., Diep, A.B., Hope, M., Promislow, D.E.L., Kennedy, S.R., Kaeberlein, M., Herr, A.J., 2019. Defining the impact of mutation accumulation on replicative lifespan in yeast using cancer-associated mutator phenotypes. Proc Natl Acad Sci U S A 116, 3062–3071. https://doi.org/10.1073/pnas.1815966116

Li, Y., Jiang, Y., Paxman, J., O'Laughlin, R., Klepin, S., Zhu, Y., Pillus, L., Tsimring, L.S., Hasty, J., Hao, N., 2020. A programmable fate decision landscape underlies single-cell aging in yeast. Science 369, 325–329. https://doi.org/10.1126/science.aax9552

Li, Y., Jin, M., O'Laughlin, R., Bittihn, P., Tsimring, L.S., Pillus, L., Hasty, J., Hao, N., 2017. Multigenerational silencing dynamics control cell aging. Proceedings of the National Academy of Sciences 114, 11253–11258. https://doi.org/10.1073/pnas.1703379114

Liu, P., Young, T.Z., Acar, M., 2015. Yeast Replicator: A High-Throughput Multiplexed Microfluidics Platform for Automated Measurements of Single-Cell Aging. Cell Reports 13, 634–644. https://doi.org/10.1016/j.celrep.2015.09.012

Longtine, M.S., Mckenzie III, A., Demarini, D.J., Shah, N.G., Wach, A., Brachat, A., Philippsen, P., Pringle, J.R., 1998. Additional modules for versatile and economical PCR-based gene deletion and modification in Saccharomyces cerevisiae. Yeast 14, 953–961. https://doi.org/10.1002/(SICI)1097-0061(199807)14:10%253C953::AID-YEA293%253E3.0.CO;2-U

Maklakov, A.A., Immler, S., 2016. The Expensive Germline and the Evolution of Ageing. Current Biology 26, R577–R586. https://doi.org/10.1016/j.cub.2016.04.012

Mochida, K., Oikawa, Y., Kimura, Y., Kirisako, H., Hirano, H., Ohsumi, Y., Nakatogawa, H., 2015. Receptor-mediated selective autophagy degrades the endoplasmic reticulum and the nucleus. Nature 522, 359–362. https://doi.org/10.1038/nature14506

Mortimer, R.K., Johnston, J.R., 1959. Life Span of Individual Yeast Cells. Nature 183, 1751–1752. https://doi.org/10.1038/1831751a0
Neiman, A.M., 2011. Sporulation in the Budding Yeast Saccharomyces cerevisiae. Genetics 189, 737–765. https://doi.org/10.1534/genetics.111.127126
Nyström, T., Liu, B., 2014. Protein quality control in time and space – links to cellular aging. FEMS Yeast Res 14, 40–48. https://doi.org/10.1111/1567-1364.12095
Okamoto, K., Kondo-Okamoto, N., Ohsumi, Y., 2009. Mitochondria-Anchored Receptor Atg32 Mediates Degradation of Mitochondria via Selective Autophagy. Developmental Cell 17, 87–97. https://doi.org/10.1016/j.devcel.2009.06.013
Otto, G.M., Brar, G.A., 2022. Developmentally regulated selective autophagy determines ER inheritance by gametes. Autophagy 18, 1732–1733. https://doi.org/10.1080/15548627.2022.2040315
Otto, G.M., Cheunkarndee, T., Leslie, J.M., Brar, G.A., 2021. Programmed cortical ER collapse drives selective ER degradation and inheritance in yeast meiosis. Journal of Cell Biology 220, e202108105. https://doi.org/10.1083/jcb.202108105
Padmore, R., Cao, L., Kleckner, N., 1991. Temporal comparison of recombination and synaptonemal complex formation during meiosis in S. cerevisiae. Cell 66, 1239–1256. https://doi.org/10.1016/0092-8674(91)90046-2
Powers, E.N., Chan, C., Doron-Mandel, E., Llacsahuanga Allcca, L., Kim Kim, J., Jovanovic, M., Brar, G.A., 2022. Bidirectional promoter activity from expression cassettes can drive off-target repression of neighboring gene translation. eLife 11, e81086. https://doi.org/10.7554/eLife.81086
Rubinsztein, D.C., Mariño, G., Kroemer, G., 2011. Autophagy and Aging. Cell 146, 682–695. https://doi.org/10.1016/j.cell.2011.07.030
Saliba, E., Evangelinos, M., Gournas, C., Corrillon, F., Georis, I., André, B., 2018. The yeast H+-ATPase Pma1 promotes Rag/Gtr-dependent TORC1 activation in response to H+-coupled nutrient uptake. eLife 7, e31981. https://doi.org/10.7554/eLife.31981
Sampaio-Marques, B., Felgueiras, C., Silva, A., Rodrigues, M., Tenreiro, S., Franssens, V., Reichert, A.S., Outeiro, T.F., Winderickx, J., Ludovico, P., 2012. SNCA (α-synuclein)-induced toxicity in yeast cells is dependent on Sir2-mediated mitophagy. Autophagy 8, 1494–1509. https://doi.org/10.4161/auto.21275
Sawyer, E.M., Joshi, P.R., Jorgensen, V., Yunus, J., Berchowitz, L.E., Ünal, E., 2018. Developmental regulation of an organelle tether coordinates mitochondrial remodeling in meiosis. J Cell Biol 218, 559–579. https://doi.org/10.1083/jcb.201807097
Schindelin, J., Arganda-Carreras, I., Frise, E., Kaynig, V., Longair, M., Pietzsch, T., Preibisch, S., Rueden, C., Saalfeld, S., Schmid, B., Tinevez, J.-Y., White, D.J., Hartenstein, V., Eliceiri, K., Tomancak, P., Cardona, A., 2012. Fiji: an open-source platform for biological-image analysis. Nature Methods 9, 676–682. https://doi.org/10.1038/nmeth.2019
Schlesser, A., Ulaszewski, S., Ghislain, M., Goffeau, A., 1988. A second transport ATPase gene in Saccharomyces cerevisiae. Journal of Biological Chemistry 263, 19480–19487. https://doi.org/10.1016/S0021-9258(19)77659-5
Serrano, R., Kielland-Brandt, M.C., Fink, G.R., 1986. Yeast plasma membrane ATPase is essential for growth and has homology with (Na+ + K+), K+- and Ca2+-ATPases. Nature 319, 689–693. https://doi.org/10.1038/319689a0
Simonsen, A., Cumming, R.C., Brech, A., Isakson, P., Schubert, D.R., Finley, K.D., 2008. Promoting basal levels of autophagy in the nervous system enhances longevity and oxidant resistance in adult Drosophila. Autophagy 4, 176–184. https://doi.org/10.4161/auto.5269

Sinclair, D.A., Guarente, L., 1997. Extrachromosomal rDNA Circles— A Cause of Aging in Yeast. Cell 91, 1033–1042. https://doi.org/10.1016/S0092-8674(00)80493-6

Sing, T.L., Brar, G.A., Ünal, E., 2022. Gametogenesis: Exploring an Endogenous Rejuvenation Program to Understand Cellular Aging and Quality Control. Annu. Rev. Genet. 56, 89–112. https://doi.org/10.1146/annurev-genet-080320-025104

Smeal, T., Claus, J., Kennedy, B., Cole, F., Guarente, L., 1996. Loss of Transcriptional Silencing Causes Sterility in Old Mother Cells of S. cerevisiae. Cell 84, 633–642. https://doi.org/10.1016/S0092-8674(00)81038-7

Smelick, C., Ahmed, S., 2005. Achieving immortality in the *C. elegans* germline. Ageing Research Reviews 4, 67–82. https://doi.org/10.1016/j.arr.2004.09.002

Suda, Y., Nakanishi, H., Mathieson, E.M., Neiman, A.M., 2007. Alternative Modes of Organellar Segregation during Sporulation in Saccharomyces cerevisiae. Eukaryotic Cell 6, 2009–2017. https://doi.org/10.1128/ec.00238-07

Thayer, N.H., Robles, M., Xu, J., Schinski, E.L., Hotz, M., Keyser, R., Millett-Sikking, A., Okreglak, V., Rogers, J.V., Waite, A.J., Wranik, B.J., York, A.G., McIsaac, R.S., Gottschling, D.E., 2022. The Yeast Lifespan Machine: a microfluidic platform for automated replicative lifespan measurements. https://doi.org/10.1101/2022.02.14.480146

Tyler, J.K., Johnson, J.E., 2018. The role of autophagy in the regulation of yeast life span. Ann N Y Acad Sci 1418, 31–43. https://doi.org/10.1111/nyas.13549

Ünal, E., Amon, A., 2011. Gamete formation resets the aging clock in yeast. Cold Spring Harb Symp Quant Biol 76, 73–80. https://doi.org/10.1101/sqb.2011.76.011379

Ünal, E., Kinde, B., Amon, A., 2011. Gametogenesis Eliminates Age-Induced Cellular Damage and Resets Life Span in Yeast. Science 332, 1554–1557. https://doi.org/10.1126/science.1204349

Williamson, D.H., Johnston, L.H., Fennell, D.J., Simchen, G., 1983. The timing of the S phase and other nuclear events in yeast meiosis. Experimental Cell Research 145, 209–217. https://doi.org/10.1016/S0014-4827(83)80022-6

Xu, L., Ajimura, M., Padmore, R., Klein, C., Kleckner, N., 1995. NDT80, a meiosis-specific gene required for exit from pachytene in Saccharomyces cerevisiae. Mol Cell Biol 15, 6572–6581. https://doi.org/10.1128/mcb.15.12.6572

Yamashita, Y.M., 2023. Asymmetric Stem Cell Division and Germline Immortality. Annual Review of Genetics 57, 181–199. https://doi.org/10.1146/annurev-genet-022123-040039